Calculations of inner-shell ionization by electron impact with the distorted-wave and plane-wave Born approximations

David Bote* and Francesc Salvat†
Facultat de Física (ECM), Universitat de Barcelona, Diagonal 647, 08028 Barcelona, Spain
(Received 24 October 2007; published 1 April 2008)

A method is described for computing total cross sections for the ionization of inner shells of atoms and positive ions by impact of electrons and positrons with arbitrary energies. The method combines the relativistic plane-wave Born approximation (PWBA) with a semirelativistic version of the distorted-wave Born approximation (DWBA). Formal expressions for the longitudinal and transverse generalized oscillator strengths (GOSs) of closed shells are derived. Tables of GOSs for *K* shells and for *L* and *M* subshells of neutral atoms have been calculated for a discrete grid of energy losses and recoil energies. A suitable interpolation scheme allows the easy evaluation of PWBA ionization cross sections from these GOS tables. The difference between the total ionization cross sections that result from the DWBA and the PWBA (considering the longitudinal interaction only) has been calculated numerically for projectiles with kinetic energies up to 16 times the ionization energy of the active shell. In this energy range, ionization cross sections with the accuracy of a distorted-wave calculation are obtained by simply adding this difference to the cross section resulting from the conventional PWBA. For higher energies, the cross section is obtained by multiplying the PWBA cross section by an energy-dependent scaling factor that is determined by a single fitted parameter. Numerical results are shown to agree with experimental data, when these are available.

DOI: 10.1103/PhysRevA.77.042701 PACS number(s): 34.80.Dp, 34.80.Uv

I. INTRODUCTION

Ionization of inner shells by electron impact is the main source of characteristic x rays from materials irradiated by energetic electron beams. Knowledge of accurate cross sections for electron-impact ionization is therefore required for a quantitative understanding of processes involving the generation of characteristic x rays by electrons, such as those found in electron-probe microanalysis and Auger electron spectroscopy, x-ray generators, radiation dosimetry, and plasma physics. These processes can be studied by means of Monte Carlo simulation of coupled electron-photon transport. The common practice in general-purpose Monte Carlo codes [1–3] is to rely on approximate cross sections evaluated from the relativistic plane-wave Born approximation (PWBA), usually with empirical low-energy corrections. The PWBA provides an accurate description of the ionization process only for electrons and positrons with kinetic energy E higher than about 30 times the ionization energy U of the active shell. Unfortunately, except for the innermost shells of heavy elements, the ionization cross section takes its larger values in the energy range where the PWBA is not accurate and where the adopted empirical corrections are known to be only roughly approximate.

It is worth mentioning that the experimental information available on electron-impact ionization is fairly limited and experimental data are frequently affected by considerable uncertainties. Data for *K*-shell ionization available up to December 1999 were compiled by Liu *et al.* [4], and only a few additional measurements have been reported since then. For most elements, *K*-shell ionization data are limited to a few electron energies and, in cases where measurements from different laboratories are available, relative differences between them usually exceed the magnitude of the estimated experimental uncertainties. Measurements for *L*-shell ionization are much less abundant and are affected by still larger uncertainties. For *M* and outer shells only very few measurements have been reported. Experimental data for ionization by positron impact are still scarcer.

On the basis of this limited experimental information, a number of empirical and semiempirical analytical formulas for evaluating electron-impact ionization cross sections have been proposed [5–8]. However, these formulas are valid only in limited energy ranges, where enough experimental information is available, and they are affected by the same uncertainties as the experimental data. Calculations of *K*- and *L*-shell ionization cross sections within the nonrelativistic PWBA have been reviewed by Powell [9,10]. More recently, Rez [11] has reported similar calculations for *K*, *L*, and also *M* shells. Scofield [12] described a fully relativistic formulation of the PWBA and gave total cross sections for *K* and *L* shells of selected elements. Approximations based on the PWBA have also been proposed by a number of authors, usually by combining analytical approximate forms of the generalized oscillator strength with phenomenological low-energy corrections. Among the most elaborate of these formulations are the binary-encounter Bethe model of Kim *et al.* [13–15] and the Deutsch-Märk formulation [16]. The Weiszäcker-Williams method of virtual quanta used by Kolvenstvedt [17], Seltzer [18], and others can also be regarded as a simplification of the PWBA (see, e.g., Ref. [19]).

As indicated above, the PWBA is reliable only for projectiles with kinetic energies well above the ionization threshold. Comparisons of triply differential cross sections calculated from the PWBA with experimental data [20–23] reveal limitations of this approximation even for energies of the

*bote@ecm.ub.es
†cesc@ecm.ub.es

order of $20U$. The observed differences are mostly caused by the neglect of the distortion of the projectile wave functions by the field of the target atom and also by the inadequate treatment of electron exchange. A more accurate theoretical description of triply differential cross sections is obtained from the relativistic distorted-wave Born approximation (DWBA), which consistently accounts for the effects of both distortion and exchange [24,25]. Various authors have reported DWBA calculations of ionization cross sections for ions [26–29]. Calculations for neutral atoms are much more difficult because of the slower convergence of the partial-wave series. Only recently, Segui *et al.* [30] and Colgan and Fontes [31] have reported semirelativistic DWBA calculations for neutral atoms. The results from these two groups are in close agreement, but limited to energies up to about $10U$. At higher energies, numerical instabilities and poor convergence of the partial-wave series render the calculation impracticable.

The aim of the present work was to devise a more efficient calculation scheme, which can enable the calculation of accurate ionization cross sections in the whole energy range of interest for Monte Carlo simulations of radiation transport. Such an scheme is obtained here by combining the conventional PWBA [32–34] with the semirelativistic DWBA [30,31]. Within the PWBA, the double-differential cross section (DDCS) is obtained as the sum of products of purely kinematical factors and structure functions [the so-called generalized oscillator strengths (GOSs)]. After calculating the GOSs, the DDCS can be easily evaluated not only for electrons, but for any charged particle (the mass, charge, and energy of the projectile appear only in the kinematical factors, and in the limits of the integrals). The key point in our computation scheme is that the distortion caused by the field of the target atom decreases when the orbital angular momentum of the projectile increases. Hence one can consider the *difference* between the DWBA and the PWBA DDCSs as a correction to the latter, in the hope that the terms of the partial-wave series of the difference will decrease faster with the orbital angular momentum than those of the corresponding DWBA series. Numerical calculations confirm this fact and reveal that the correction can be evaluated accurately for energies up to about $25U$, i.e., the numerical convergence interval is about 2.5 wider than that of the DWBA series. DWBA cross sections have been calculated in this manner for projectiles with energies up to $16U$ and for the K shell and L and M subshells of the atoms from hydrogen ($Z=1$) to einsteinium ($Z=99$). For energies between $16U$ and $25U$, the program does converge, but the calculations take much longer times. The difference between the PWBA and the DWBA total ionization cross sections varies smoothly with the energy of the projectile and, for energies above the cross section maximum, its magnitude decreases rapidly for increasing energies. Although the DWBA accounts for exchange effects in a consistent way, it is difficult to make allowance for these effects within the relativistic PWBA. For nonrelativistic projectile electrons, exchange effects may be described using the approximation proposed by Ochkur [35] (see also [36]). Unfortunately, a generalization of Ochkur's method to the relativistic theory does not seem possible.

We have found that for energies higher than $\sim 16U$ the DWBA cross section can be closely approximated by the PWBA cross section multiplied by a scaling factor of the form $E/(E+bU)$, where the parameter b is independent of the energy. This kind of scaling correction has been suggested by various authors (e.g., [19,37]) to approximately account for the increase in the effective kinetic energy of the projectile caused by the atomic potential. The scaling parameter b is here determined by matching the calculated DWBA cross section at $E=16U$ with the "scaled" PWBA. The scaled PWBA then allows the easy calculation of ionization cross sections for projectiles with energies higher than $16U$. Summarizing, the present ionization cross sections are calculated by combining the DWBA for projectiles with energies up to $16U$ with the scaled PWBA for higher energies; this composite calculation scheme will be referred to as the corrected PWBA (CPWBA).

The present paper is organized as follows. Section II is devoted to basic aspects of the theory of ionizing collisions of charged particles. In Sec. III we derive general expressions for the DDCS in the PWBA, we present closed formulas for both the longitudinal and transverse GOSs and we describe an algorithm for accurate interpolation of these functions. A formal expression for the difference between the DWBA and PWBA, in the form of a partial-wave series, is derived in Sec. IV, where the numerical convergence of this series and that of the pure DWBA are also analyzed. Section V describes the CPWBA and the practical algorithm used to evaluate the ionization cross sections. In Sec. VI, our calculated ionization cross sections are compared with experimental data. Section VII contains some concluding remarks. For the sake of completeness, a brief description of the notation used to represent Dirac plane waves and spherical waves is given in Appendix A.

II. THEORY OF IONIZING COLLISIONS

Following Fano [33], we shall use the transverse (Coulomb) gauge for the electromagnetic potentials, not only because it makes the nonrelativistic limit almost trivial, but also because the DCS for the longitudinal interaction can be expressed in the same form as in the semirelativistic DWBA [30]. This last peculiarity will be used in Sec. IV to devise an improved numerical procedure for computing ionization cross sections within the DWBA. We consider collisions of a projectile electron or positron with a neutral atom or positive ion of the element of atomic number Z that result in the ionization of an inner shell of the latter. With obvious modifications, the theory can also be used to describe impact ionization by other spin-$\frac{1}{2}$ charged particles.

The effective interaction $\mathcal{H}_{\rm int}(0,1)$ between a charged Dirac particle "0" (the projectile) and a target electron "1" can be expressed in the form (see Ref. [33])

$$\mathcal{H}_{\rm int}(0,1) = -\frac{Z_0 e^2}{|\mathbf{r}-\mathbf{r}_0|} + \frac{Z_0 e^2}{2\pi^2}\int d\mathbf{q}\,\frac{\tilde{\boldsymbol{\alpha}}_0\cdot\tilde{\boldsymbol{\alpha}} - (\tilde{\boldsymbol{\alpha}}_0\cdot\hat{\mathbf{q}})(\tilde{\boldsymbol{\alpha}}\cdot\hat{\mathbf{q}})}{q^2-(W/\hbar c)^2} \times \exp[i\mathbf{q}\cdot(\mathbf{r}-\mathbf{r}_0)], \quad (1)$$

where $Z_0 e$ is the charge of the projectile ($Z_0=-1$ for electrons, +1 for positrons), $\tilde{\boldsymbol{\alpha}}_0$ and $\tilde{\boldsymbol{\alpha}}$ are the Dirac matrices, Eq. (A2), and $\mathbf{r}_0$ and $\mathbf{r}$ are the position coordinates for the pro-

jectile and the target electron, respectively. W is the energy exchanged in the course of the interaction, and $\hat{\mathbf{q}}$ is the unit vector in the direction of $\mathbf{q}$. The first term on the right-hand side of Eq. (1) is the instantaneous Coulomb interaction. The second term accounts for the exchange of virtual photons in the lowest nonvanishing perturbation order, and is usually referred to as the transverse interaction. Because the contribution from each $\tilde{\boldsymbol{\alpha}}$ factor is of the order of v/c, where v is the velocity of the particle and c is the speed of light in vacuum, the effect of the transverse interaction is expected to be appreciable only for projectiles with relativistic velocities.

Ionization cross sections will be evaluated within a theoretical framework similar to the one described in Ref. [30]. We assume that the mass of the target atom is much larger than the electron mass and we compute the cross sections in the laboratory reference frame, where the target atom is at rest. The independent-electron approximation is adopted to describe the initial and final states of the target atom, which are represented by Slater determinants $\Psi(1,\ldots,Z)$ built with Z one-electron orbitals. These orbitals are eigenfunctions of the Dirac Hamiltonian for an electron in a central potential $V_{\mathrm{T}}(r)$ (see Appendix A),

$$[c\tilde{\boldsymbol{\alpha}}\cdot\mathbf{p}+(\tilde{\beta}-1)m_ec^2+V_{\mathrm{T}}(r)]\psi_{n\kappa m}(\mathbf{r})=\epsilon_{n\kappa}\psi_{n\kappa m}(\mathbf{r}), \quad (2)$$

where $\epsilon_{n\kappa}$ is the energy of the electron, exclusive of the rest energy, and m_e is the electron mass. The interaction with the projectile causes the excitation of the target atom, which is initially in its ground state, to final states where one of the atomic electrons is free. It is convenient to use the same potential for the initial and final atomic states, because this ensures orthogonality of the one-electron orbitals and allows large simplifications of the transition matrix elements, as well as a consistent description of exchange effects in the case of electron scattering. As in Ref. [30], the potential $V_{\mathrm{T}}(r)$ is set equal to the self-consistent Dirac-Fock-Slater (DFS) potential (with Latter's tail correction [38,39]) of the neutral atom, $V^{(\mathrm{DFS})}(r)$. A practical reason for this choice is that, for inner shells with ionization energies higher than about 200 eV, the eigenvalues of the one-electron Dirac equation with the DFS potential are very close to the experimental shell ionization energies [40]. In the following, we shall set $U=-\epsilon_{n\kappa}$.

The Hamiltonian of the system (projectile and target atom) can be expressed as

$$\mathcal{H}(0,1,\ldots,Z)=\mathcal{H}_{\mathrm{T}}(1,\ldots,Z)+\mathcal{H}_{\mathrm{P}}(0)+\mathcal{H}'(0,1,\ldots,Z), \quad (3)$$

where $\mathcal{H}_{\mathrm{T}}$ and $\mathcal{H}_{\mathrm{P}}$ are the Hamiltonians of the target atom and of the free projectile respectively, and the term $\mathcal{H}'$ describes the interaction between them. In its simplest formulation, the DWBA can be obtained as follows. We rewrite the Hamiltonian (3) in the form

$$\mathcal{H}(0,1,\ldots,Z)=\mathcal{H}_{\mathrm{T}}(1,\ldots,Z)+[\mathcal{H}_{\mathrm{P}}(0)+V_{\mathrm{P}}(r_0)]+\mathcal{H}'' \quad (4)$$

with $\mathcal{H}''=\mathcal{H}'-V_{\mathrm{P}}(r_0)$. That is, we have added and subtracted an arbitrary central potential $V_{\mathrm{P}}(r_0)$ that depends only on the coordinates of the projectile. In the DWBA, the states $\psi(0)$ of the projectile before and after the collision are represented by Dirac distorted plane waves, Eq. (A20), which are exact solutions of the Dirac equation (2) for the central potential $V_{\mathrm{P}}(r_0)$. We can then consider $\mathcal{H}''$ as a perturbation that causes transitions between the eigenstates $\psi(0)\Psi(1,\ldots,N)$ of the "unperturbed" Hamiltonian $\mathcal{H}_{\mathrm{T}}+[\mathcal{H}_{\mathrm{P}}+V_{\mathrm{P}}]$. The effectiveness of the DWBA lies in the fact that $\mathcal{H}''$ can be made weaker than the original interaction $\mathcal{H}'$. Unfortunately, since the interaction $\mathcal{H}'$ does depend on the coordinates of the atomic electrons, $\mathcal{H}''$ cannot be reduced to zero. Nonetheless, it is assumed that, with a proper choice of the distorting potential V_{P}, $\mathcal{H}''$ can be made small enough to be treated as a perturbation to first order. In the present DWBA calculations, we follow the approach used in Ref. [30] and set

$$V_{\mathrm{P}}(r_0)=\begin{cases}V^{(\mathrm{DFS})}(r_0) & \text{for electrons,}\\ -V^{(\mathrm{DFS})}(r_0) & \text{for positrons.}\end{cases} \quad (5)$$

When atomic states are described within the independent-electron approximation, the only allowed transitions of the target atom are single-electron excitations, i.e., transitions to final states (Slater determinants) that differ from the ground state by a single orbital. For these transitions, the transition (T) matrix elements take the same form as for the case of one-electron atoms, i.e., we end up in the one-active-electron approximation employed in Ref. [30].

We consider that before the interaction the projectile moves with velocity $\mathbf{v}$, linear momentum $\mathbf{p}=\hbar\mathbf{k}$, and kinetic energy E; the corresponding values after the collision are $\mathbf{v}'$, $\mathbf{p}'=\hbar\mathbf{k}'$, and E', respectively. The cross section for ionizing collisions, in which the active electron is removed from the bound orbital $\psi_{n_a\kappa_a m_a}$ in a shell $(n_a\kappa_a)$ and emitted with momentum $\hbar\mathbf{k}_b$, energy ϵ_b, and in the spin state $\chi_{m_{\mathrm{S}b}}$, is given by (see, e.g., [41])

$$d\sigma=\frac{(2\pi)^4}{\hbar v}|T_{ba}|^2\delta(E-E'-\epsilon_b+\epsilon_{n_a\kappa_a})d\mathbf{k}'d\mathbf{k}_b, \quad (6)$$

where

$$T_{ba}=\langle\psi^{(-)}_{\mathbf{k}'m_{\mathrm{S}'}}(0)\psi^{(-)}_{\mathbf{k}_bm_{\mathrm{S}b}}(1)|\mathcal{H}_{\mathrm{int}}(0,1)|\psi^{(+)}_{\mathbf{k}m_{\mathrm{S}}}(0)\psi_{n_a\kappa_am_a}(1)\rangle \quad (7)$$

is the transition matrix element obtained within the one-active-electron approximation. The distorted wave functions of the final and initial states of the projectile, and of the final state of the target electron are denoted, respectively, by $\psi^{(-)}_{\mathbf{k}'m_{\mathrm{S}'}}(0)$, $\psi^{(+)}_{\mathbf{k}m_{\mathrm{S}}}(0)$, and $\psi^{(-)}_{\mathbf{k}_bm_{\mathrm{S}b}}(1)$. Note that expression (6) applies only when free states are normalized in the wave-vector scale [see Eq. (A22)]. Introducing the expression

$$d\mathbf{k}'=k'^2\frac{dk'}{dE'}dE'd\hat{\mathbf{k}}'=k'\frac{E'+m_ec^2}{c^2\hbar^2}dE'd\hat{\mathbf{k}}', \quad (8)$$

and the equivalent one for $\mathbf{k}_b$, and integrating over ϵ_b we obtain

$$d\sigma = \frac{(2\pi)^4}{\hbar v} k' k_b \frac{E' + m_e c^2}{c^2\hbar^2} \frac{\epsilon_b + m_e c^2}{c^2\hbar^2} |T_{ba}|^2 dE' d\hat{\mathbf{k}}' d\hat{\mathbf{k}}_b, \tag{9}$$

where the T-matrix elements are on the energy shell ($E + \epsilon_{n_a\kappa_a} = E' + \epsilon_b$). That is, the final energies of the projectile and the ejected electron are $E' = E - W$ and $\epsilon_b = W + \epsilon_{n_a\kappa_a} = W - U$, where W is the energy lost by the projectile.

In the following, we shall limit our considerations to the case of ionization of closed shells $n_a\kappa_a$, with $2|\kappa_a| = 2j_a + 1$ electrons. Except in very special studies, the incident beam is unpolarized, final spin states are not observed, and we do not distinguish between ionizations of the various orbitals $\psi_{n_a\kappa_a m_a}$ in the active shell. Under these circumstances, the DDCS for ionization of the $n_a\kappa_a$ shell is obtained by averaging over initial degenerate magnetic states and summing over final spin states. On the other hand, in most practical cases the ejected target electron is not observed and only the effect of the interactions on the projectile is of interest. The ionization DDCS for the closed shell is then obtained by integrating over the direction $\hat{\mathbf{k}}_b$ of the ejected electron,

$$\frac{d\sigma}{dW\, d\hat{\mathbf{k}}'} = \frac{(2\pi)^4}{\hbar v} k' k_b \frac{E - W + m_e c^2}{c^2\hbar^2} \frac{\epsilon_{n_a\kappa_a} + W + m_e c^2}{c^2\hbar^2} \int d\hat{\mathbf{k}}_b \sum_{m_{Sb}, m_a} \frac{1}{2} \sum_{m_{S'}, m_S} |T_{ba}|^2. \tag{10}$$

To perform the integration over $\hat{\mathbf{k}}_b$, we expand the distorted plane wave (DPW) $\psi^{(-)}_{\mathbf{k}_b m_{Sb}}$ in terms of spherical waves, Eq. (A10). Using the orthogonality and completeness properties of the Pauli spinors χ_μ and of the spherical spinors $\Omega_{\kappa m}(\hat{\mathbf{r}})$, we obtain

$$\frac{d\sigma}{dW\, d\hat{\mathbf{k}}'} = \frac{(2\pi)^4}{\hbar v} k' \frac{E - W + m_e c^2}{c^2\hbar^2} \frac{\epsilon_{n_a\kappa_a} + W + 2m_e c^2}{c^2\hbar^2 k_b \pi} \sum_{\kappa_b, m_b} \sum_{m_a} \frac{1}{2} \sum_{m_{S'}, m_S} |T^{(s)}_{ba}|^2, \tag{11}$$

where

$$T^{(s)}_{ba} = \langle \psi^{(-)}_{\mathbf{k}' m_{S'}}(0) \psi_{\epsilon_b \kappa_b m_b}(1) | \mathcal{H}_{\text{int}}(0,1) | \psi^{(+)}_{\mathbf{k} m_S}(0) \psi_{n_a\kappa_a m_a}(1) \rangle \tag{12}$$

is the T-matrix element corresponding to a transition of the active electron from its initial orbital to a final state represented as a spherical wave. The energy-loss DCS is obtained by integrating over final directions of the projectile,

$$\frac{d\sigma}{dW} = \int \frac{d\sigma}{dW\, d\hat{\mathbf{k}}'} d\hat{\mathbf{k}}'. \tag{13}$$

Although the present calculations are formulated for free neutral atoms and positive ions, the results are expected to be also approximately valid for atoms in molecules and in condensed media, provided only that the energy transfer W exceeds the ionization energy by some hundred eV. Aggregation effects, analogous to the fine structure observed in the absorption of x rays (see, e.g., Ref. [42]), would introduce an oscillatory component in the DCS, with a much lower impact on the ionization cross sections. It should also be mentioned that, when the target atoms are in a condensed medium, the dielectric polarizability of the medium effectively screens the distant interactions and causes a reduction of the ionization cross section of high-energy particles, which is known as the Fermi density effect. This effect has been intensively studied (see, e.g., [33,43,44] and references therein) because it produces a substantial reduction of the stopping power of relativistic charged particles. A detailed analysis of the density effect on the ionization cross sections is outside the scope of the present work, since it would require knowledge of the dielectric function of the medium which, for nonmagnetic materials, depends on the wave number and frequency of the exchanged photon. A simple method to account approximately for this effect is described by Scofield [12]; his calculations indicate that the effect on the ionization cross sections of inner shells is appreciable only at very high energies (E larger than about 100 MeV for ionization of the K shell of silver).

III. PLANE-WAVE BORN APPROXIMATION

In the relativistic version of the PWBA the projectile wave functions are approximated by Dirac plane waves, i.e., the distortion caused by the field of the target atom is neglected. It is worth noting that, in the limit where the distorting potential vanishes, i.e., $V_P \to 0$, the distorted waves reduce to plane waves and, therefore, the DWBA reduces to the PWBA. Traditionally, the PWBA has been employed as the basis of the theory of stopping of fast charged particles (see Refs. [32–34] and references therein), and leads to the celebrated formula of Bethe for the collision stopping power of high-energy particles. The first systematic calculations of total cross sections for inner-shell ionization by electron impact within the relativistic PWBA were performed by Scofield [12], who calculated the cross sections for the K shell and L subshells of eight elements, with atomic numbers distributed almost uniformly between argon ($Z=18$) and ura-

nium ($Z=92$). In the present paper, we adopt a different calculation scheme, which leads to an exact expression for the DDCS in terms of the relativistic (longitudinal and transverse) generalized oscillator strengths. Although our treatment is similar to that of Fano [33] for heavy charged particles, we avoid the assumption expressed by Eq. (7) in Ref. [33], which does not hold for projectiles with the mass of the electron.

In the PWBA the DDCS for impact ionization is given by Eqs. (11) and (12), but with the distorted waves of the projectile replaced by plane waves,

$$\phi_{\mathbf{k},m_S,+1}(\mathbf{r}) = \frac{e^{i\mathbf{k}\cdot\mathbf{r}}}{(2\pi)^{3/2}} U_{\mathbf{k},m_S,+1}. \tag{14}$$

Introducing the Fourier transform of the Coulomb potential, we can write

$$\mathcal{H}_{\rm int}(0,1) = -\frac{Z_0 e^2}{2\pi^2}\int d\mathbf{q}\left(\frac{1}{q^2} - \frac{\tilde{\boldsymbol{\alpha}}_0\cdot\tilde{\boldsymbol{\alpha}} - (\tilde{\boldsymbol{\alpha}}_0\cdot\hat{\mathbf{q}})(\tilde{\boldsymbol{\alpha}}\cdot\hat{\mathbf{q}})}{q^2 - (W/\hbar c)^2}\right) \times \exp[i\mathbf{q}\cdot(\mathbf{r}-\mathbf{r}_0)], \tag{15}$$

and the transition matrix element (12) takes the form

$$T_{ba}^{(\rm PWs)} = -\frac{Z_0 e^2}{2\pi^2}\int d\mathbf{q}\int d\mathbf{r}_0\int d\mathbf{r}\,\phi^\dagger_{\mathbf{k}',m_{S'},+1}(\mathbf{r}_0) \times \psi^\dagger_{\epsilon_b\kappa_b m_b}(\mathbf{r})\left(\frac{1}{q^2} - \frac{\tilde{\boldsymbol{\alpha}}_0\cdot\tilde{\boldsymbol{\alpha}} - (\tilde{\boldsymbol{\alpha}}_0\cdot\hat{\mathbf{q}})(\tilde{\boldsymbol{\alpha}}\cdot\hat{\mathbf{q}})}{q^2 - (W/\hbar c)^2}\right) \times \exp[i\mathbf{q}\cdot(\mathbf{r}-\mathbf{r}_0)]\phi_{\mathbf{k},m_S,+1}(\mathbf{r}_0)\psi_{n_a\kappa_a m_a}(\mathbf{r}). \tag{16}$$

Integration over the space variables of the projectile ("0") is elementary; the result contains the delta function $\delta(\mathbf{q}-\mathbf{k}-\mathbf{k}')$ as a global factor. Integration over $\mathbf{q}$ then gives

$$T_{ba}^{(\rm PWs)} = -\frac{Z_0 e^2}{2\pi^2}\int d\mathbf{r}\, U^\dagger_{\mathbf{k}',m_{S'},+1}\psi^\dagger_{\epsilon_b\kappa_b m_b}(\mathbf{r}) \times\left(\frac{1}{q^2} - \frac{\tilde{\boldsymbol{\alpha}}_0\cdot\tilde{\boldsymbol{\alpha}} - (\tilde{\boldsymbol{\alpha}}_0\cdot\hat{\mathbf{q}})(\tilde{\boldsymbol{\alpha}}\cdot\hat{\mathbf{q}})}{q^2 - (W/\hbar c)^2}\right) \times \exp(i\mathbf{q}\cdot\mathbf{r})U_{\mathbf{k},m_S,+1}\psi_{n_a\kappa_a m_a}(\mathbf{r}). \tag{17}$$

From now on, $\hbar\mathbf{q}=\hbar\mathbf{k}-\hbar\mathbf{k}'$ is the momentum transferred to the target electron.

It is worth mentioning that the present treatment is strictly equivalent to that of Bethe [32,45]. This is easily seen by noting that the Dirac equation for plane waves [i.e., Eq. (A3) with $V=0$] implies that

$$[c\hbar\tilde{\boldsymbol{\alpha}}\cdot\mathbf{k} + (\tilde{\beta}-1)m_e c^2]U_{\mathbf{k},m_S,+1} = EU_{\mathbf{k},m_S,+1} \tag{18}$$

and, therefore,

$$\begin{aligned}(c\hbar\tilde{\boldsymbol{\alpha}}\cdot\mathbf{q})U_{\mathbf{k},m_S,+1} &= \{[c\hbar\tilde{\boldsymbol{\alpha}}\cdot\mathbf{k} + (\tilde{\beta}-1)m_e c^2] \\ &\quad - [c\hbar\tilde{\boldsymbol{\alpha}}\cdot\mathbf{k}' - (\tilde{\beta}-1)m_e c^2]\} \\ &\quad \times U_{\mathbf{k},m_S,+1} \\ &= (E-E')U_{\mathbf{k},m_S,+1} = WU_{\mathbf{k},m_S,+1}.\end{aligned} \tag{19}$$

Hence,

$$\left(\frac{1}{q^2} - \frac{\tilde{\boldsymbol{\alpha}}_0\cdot\tilde{\boldsymbol{\alpha}} - (\tilde{\boldsymbol{\alpha}}_0\cdot\hat{\mathbf{q}})(\tilde{\boldsymbol{\alpha}}\cdot\hat{\mathbf{q}})}{q^2 - (W/\hbar c)^2}\right)U_{\mathbf{k},m_S,+1} = \frac{1-\tilde{\boldsymbol{\alpha}}_0\cdot\tilde{\boldsymbol{\alpha}}}{q^2-(W/\hbar c)^2}U_{\mathbf{k},m_S,+1}, \tag{20}$$

and the T-matrix element (17) can be cast in the form

$$T_{ba}^{(\rm PWs)} = -\frac{Z_0 e^2}{2\pi^2}\frac{1}{q^2-(W/\hbar c)^2}\int d\mathbf{r}\;\psi^\dagger_{\epsilon_b\kappa_b m_b}(\mathbf{r}) \times (A_0 + \mathbf{A}\cdot\tilde{\boldsymbol{\alpha}})\exp(i\mathbf{q}\cdot\mathbf{r})\psi_{n_a\kappa_a m_a}(\mathbf{r}), \tag{21}$$

where

$$A_0 = U^\dagger_{\mathbf{k}',m_{S'},+1}U_{\mathbf{k},m_S,+1}, \tag{22a}$$

$$\mathbf{A} = -U^\dagger_{\mathbf{k}',m_{S'},+1}\tilde{\boldsymbol{\alpha}}_0 U_{\mathbf{k},m_S,+1}. \tag{22b}$$

Expression (21) agrees exactly with the matrix elements in Bethe's formulation, Eq. (5) of [45] and Eq. (50.1) of [32].

For the purposes of the present work, it is more expedient to express the transition matrix element [see Eq. (17)] in the form

$$\begin{aligned}T_{ba}^{(\rm PWs)} = -\frac{Z_0 e^2}{2\pi^2}\Bigg\{ & U^\dagger_{\mathbf{k}',m_{S'},+1}U_{\mathbf{k},m_S,+1}\frac{1}{q^2} \\ & \times\langle\psi_{\epsilon_b\kappa_b m_b}|\exp(i\mathbf{q}\cdot\mathbf{r})|\psi_{n_a\kappa_a m_a}\rangle \\ & - U^\dagger_{\mathbf{k}',m_{S'},+1}\left(\tilde{\boldsymbol{\alpha}}_0 - \frac{W}{c\hbar q^2}\mathbf{q}\right)U_{\mathbf{k},m_S,+1} \\ & \times\frac{\langle\psi_{\epsilon_b\kappa_b m_b}|\tilde{\boldsymbol{\alpha}}\exp(i\mathbf{q}\cdot\mathbf{r})|\psi_{n_a\kappa_a m_a}\rangle}{q^2-(W/c\hbar)^2}\Bigg\}.\end{aligned} \tag{23}$$

We note that the operators in the longitudinal and transverse terms have different parities under reflection on any plane that contains $\mathbf{q}$. As the spherical waves also have definite parity under these reflections, it follows that, for a given transition, the transverse and longitudinal terms cannot be different from zero simultaneously. That is, the longitudinal and transverse interactions excite transitions of the active electron from its initial bound orbital to final orbitals of different parities and do not interfere. Therefore,

$$\begin{aligned}|T_{ba}^{(\rm PWs)}|^2 = & \frac{Z_0^2 e^4}{4\pi^4}\frac{1}{q^4}|U^\dagger_{\mathbf{k}',m_{S'},+1}U_{\mathbf{k},m_S,+1}|^2 \\ & \times|\langle\psi_{\epsilon_b\kappa_b m_b}|\exp(i\mathbf{q}\cdot\mathbf{r})|\psi_{n_a\kappa_a m_a}\rangle|^2 \\ & + \frac{Z_0^2 e^4}{4\pi^4}\frac{1}{[q^2-(W/c\hbar)^2]^2}\Bigg| U^\dagger_{\mathbf{k}',m_{S'},+1} \\ & \times\left(\tilde{\boldsymbol{\alpha}}_0 - \frac{W}{c\hbar q^2}\mathbf{q}\right)\cdot\mathbf{D}U_{\mathbf{k},m_S,+1}\Bigg|^2.\end{aligned} \tag{24}$$

with

$$\mathbf{D} \equiv \langle\psi_{\epsilon_b\kappa_b m_b}|\tilde{\boldsymbol{\alpha}}\exp(i\mathbf{q}\cdot\mathbf{r})|\psi_{n_a\kappa_a m_a}\rangle. \tag{25}$$

This clean separation of longitudinal and transverse contributions occurs only when the active target electron moves in

a spherical potential. Any departure from spherical symmetry would induce interference between the longitudinal and transverse interactions [46].

To evaluate the DDCS it is convenient to perform the various summations in the order in which they appear in Eq. (11). The spin-averaged squared matrix element

$$\mathcal{T}_1 \equiv \frac{1}{2}\sum_{m_{S'},m_S} |T_{ba}^{(\mathrm{PWs})}|^2 \tag{26}$$

can be expressed in the form

$$\mathcal{T}_1 = \frac{Z_0^2 e^4}{4\pi^4}\frac{1}{q^4}|\langle \psi_{\epsilon_b \kappa_b m_b}|\exp(i\mathbf{q}\cdot\mathbf{r})|\psi_{n_a\kappa_a m_a}\rangle|^2 \mathcal{S}_\mathrm{L} + \frac{Z_0^2 e^4}{4\pi^4}\frac{1}{[q^2-(W/c\hbar)^2]^2}\mathcal{S}_\mathrm{T}, \tag{27}$$

where

$$\mathcal{S}_\mathrm{L} \equiv \frac{1}{2}\sum_{m_{S'},m_S} |U^\dagger_{\mathbf{k}',m_{S'},+1}U_{\mathbf{k},m_S,+1}|^2 \tag{28}$$

and

$$\mathcal{S}_\mathrm{T} \equiv \frac{1}{2}\sum_{m_{S'},m_S} \left| U^\dagger_{\mathbf{k}',m_{S'},+1}\left(\tilde{\boldsymbol{\alpha}}_0 - \frac{W}{c\hbar q^2}\mathbf{q}\right)\cdot\mathbf{D}U_{\mathbf{k},m_S,+1}\right|^2. \tag{29}$$

The summations in Eqs. (28) and (29) can be evaluated by using conventional projection tricks (see, e.g., Ref. [47]). The calculation is easier for the longitudinal term,

$$\mathcal{S}_\mathrm{L} = \frac{1}{2}\sum_{m_{S'}} U^\dagger_{\mathbf{k}',m_{S'},+1}\left(\sum_{m_S} U_{\mathbf{k},m_S,+1}U^\dagger_{\mathbf{k},m_S,+1}\right)U_{\mathbf{k}',m_{S'},+1} = \frac{1}{2}\sum_{m_{S'}} U^\dagger_{\mathbf{k}',m_{S'},+1}\Pi_{\mathbf{k},+1}U_{\mathbf{k}',m_{S'},+1}, \tag{30}$$

where we have introduced the projector $\Pi_{\mathbf{k},+1}$ on the positive-energy subspace, Eq. (A9). To evaluate the expression (30), we replace the spinors $U_{\mathbf{k}',m_{S'},+1}$ by $\Pi_{\mathbf{k}',+1}U_{\mathbf{k}',m_{S'},\tau}$ and extend the summation to positive- and negative-energy spinors. We thus have

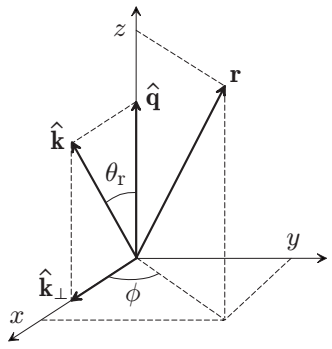

FIG. 1. Reference frame used in the evaluation of the PWBA transition matrix elements.

$$\mathcal{S}_\mathrm{L} = \frac{1}{2}\sum_{m_{S'},\tau} U^\dagger_{\mathbf{k}',m_{S'},\tau}\Pi_{\mathbf{k}',+1}\Pi_{\mathbf{k},+1}\Pi_{\mathbf{k}',+1}U_{\mathbf{k}',m_{S'},\tau} = \frac{1}{2}\mathrm{Tr}\{\Pi_{\mathbf{k}',+1}\Pi_{\mathbf{k},+1}\Pi_{\mathbf{k}',+1}\}, \tag{31}$$

where the symbol Tr stands for the trace (the sum of diagonal elements) of the matrix, which is a sum of products of Dirac matrices. This trace can be readily calculated by using the method described, e.g., in Heitler's book [47]. The final result is

$$\mathcal{S}_\mathrm{L} = \frac{(2E-W+2m_ec^2)^2-(c\hbar q)^2}{4(E+m_ec^2)(E-W+m_ec^2)}. \tag{32}$$

The transverse term can be evaluated similarly, although the calculation is much more laborious. The result can be expressed in the following, relatively compact form:

$$\mathcal{S}_\mathrm{T} = \frac{E+m_ec^2}{E-W+m_ec^2}\left(\beta^2|\hat{\mathbf{k}}_\perp\cdot\mathbf{D}_\perp|^2 + \frac{(c\hbar q)^2-W^2}{4(E+m_ec^2)^2}|\mathbf{D}_\perp|^2\right), \tag{33}$$

where $\beta=v/c$, $\mathbf{D}_\perp=\mathbf{D}-(\mathbf{D}\cdot\hat{\mathbf{q}})\hat{\mathbf{q}}$ is the "transverse" component of the vector $\mathbf{D}$ (i.e., the component perpendicular to the momentum transfer $\mathbf{q}$), and $\hat{\mathbf{k}}_\perp=\hat{\mathbf{k}}-(\hat{\mathbf{k}}\cdot\hat{\mathbf{q}})\hat{\mathbf{q}}$ (Fig. 1).

Continuing with the evaluation of the DDCS, Eq. (11), we can now include the summations over m_a, κ_b, and m_b and calculate the quantity

$$\mathcal{T}_2 \equiv \sum_{\kappa_b,m_b}\sum_{m_a}\frac{1}{2}\sum_{m_{S'},m_S}|T_{ba}^{(\mathrm{PWs})}|^2 = \sum_{\kappa_b,m_b}\sum_{m_a}\mathcal{T}_1 = \frac{Z_0^2e^4}{4\pi^4}\frac{1}{q^4}\frac{(2E-W+2m_ec^2)^2-(c\hbar q)^2}{4(E+m_ec^2)(E-W+m_ec^2)}\sum_{\kappa_b,m_b}\sum_{m_a}|\langle\psi_{\epsilon_b\kappa_bm_b}|\exp(i\mathbf{q}\cdot\mathbf{r})|\psi_{n_a\kappa_am_a}\rangle|^2$$
$$+\frac{Z_0^2e^4}{4\pi^4}\frac{1}{[q^2-(W/c\hbar)^2]^2}\frac{E+m_ec^2}{E-W+m_ec^2}\sum_{\kappa_b,m_b}\sum_{m_a}\left(\beta^2|\hat{\mathbf{k}}_\perp\cdot\mathbf{D}_\perp|^2+\frac{(c\hbar q)^2-W^2}{4(E+m_ec^2)^2}|\mathbf{D}_\perp|^2\right). \tag{34}$$

For the evaluation of the matrix elements, it is convenient to select a reference frame with the z axis in the direction of $\mathbf{q}$ and the x axis parallel to $\hat{\mathbf{k}}_\perp$ (see Fig. 1). Noting the axial symmetry of the system about this z axis, we can write

$$\mathcal{T}_2 = \frac{Z_0^2 e^4}{4\pi^4}\frac{1}{q^4}\frac{(2E - W + 2m_e c^2)^2 - (c\hbar q)^2}{4(E + m_e c^2)(E - W + m_e c^2)}\sum_{\kappa_b, m_b}\sum_{m_a}|\langle\psi_{\epsilon_b\kappa_b m_b}|\exp(i\mathbf{q}\cdot\mathbf{r})|\psi_{n_a\kappa_a m_a}\rangle|^2$$
$$+\frac{Z_0^2 e^4}{4\pi^4}\frac{1}{[q^2 - (W/c\hbar)^2]^2}\frac{E + m_e c^2}{E - W + m_e c^2}\left(\beta^2\sin^2\theta_r + \frac{(c\hbar q)^2 - W^2}{2(E + m_e c^2)^2}\right)\sum_{\kappa_b, m_b}\sum_{m_a}|D_x|^2, \tag{35}$$

where we have introduced the "recoil angle" θ_r, the angle between the vectors $\hat{\mathbf{k}}$ and $\hat{\mathbf{q}}$ (see Fig. 1), which is given by

$$\cos\theta_r = \frac{W}{\beta(c\hbar q)}\left(1 + \frac{(c\hbar q)^2 - W^2}{2W(E + m_e c^2)}\right). \tag{36}$$

This formula results directly from squaring the identity $\mathbf{k} - \mathbf{q} = \mathbf{k}'$.

Following Fano [33], we introduce the recoil energy Q, defined by

$$Q(Q + 2m_e c^2) = (c\hbar q)^2 = c^2\hbar^2(k^2 + k'^2 - 2kk'\cos\theta), \tag{37}$$

i.e., Q is the kinetic energy of a free electron that moves with momentum $\hbar q$. In the case of binary collisions of the projectile with free electrons at rest we have $Q = W$, because the energy lost by the projectile is equal to the kinetic energy of the recoiling target electron. The DDCS takes a simpler and more convenient form when it is considered as a function of the recoil energy instead of the angular deflection $\hat{\mathbf{k}}'$. Inserting the result (35) into the right-hand side of Eq. (11), after simple algebraical manipulations, we obtain the following expression for the ionization DDCS:

$$\frac{d\sigma^{(\mathrm{PW})}}{dW\,dQ} = \frac{d\sigma}{dW\,d\hat{\mathbf{k}}'}\frac{2\pi(Q + m_e c^2)}{c^2\hbar^2 kk'} = \frac{2\pi Z_0^2 e^4}{m_e v^2}\left\{\frac{2m_e c^2}{WQ(Q + 2m_e c^2)}\left(\frac{(2E - W + 2m_e c^2)^2 - Q(Q + 2m_e c^2)}{4(E + m_e c^2)^2}\right)\frac{df_{n_a\kappa_a}(Q, W)}{dW}\right.$$
$$\left.+\frac{2m_e c^2 W}{[Q(Q + 2m_e c^2) - W^2]^2}\left[\beta^2\sin^2\theta_r + \left(\frac{Q(Q + 2m_e c^2) - W^2}{2(E + m_e c^2)^2}\right)\right]\frac{dg_{n_a\kappa_a}(Q, W)}{dW}\right\}, \tag{38}$$

where we have introduced the longitudinal generalized oscillator strength (GOS), defined by

$$\frac{df_{n_a\kappa_a}(Q, W)}{dW} \equiv \frac{W2(Q + m_e c^2)}{Q(Q + 2m_e c^2)}\frac{k_b}{(\epsilon_{n_a\kappa_a} + W)\pi}\sum_{m_a}\sum_{\kappa_b, m_b}|\langle\psi_{\epsilon_b\kappa_b m_b}|\exp(i\mathbf{q}\cdot\mathbf{r})|\psi_{n_a\kappa_a m_a}\rangle|^2, \tag{39}$$

and the transverse generalized oscillator strength (TGOS), defined as follows:

$$\frac{dg_{n_a\kappa_a}(Q, W)}{dW} \equiv \frac{2(Q + m_e c^2)}{W}\frac{k_b}{(\epsilon_{n_a\kappa_a} + W)\pi}\sum_{m_a}\sum_{\kappa_b, m_b}|\langle\psi_{\epsilon_b\kappa_b m_b}|\tilde{\alpha}_x\exp(i\mathbf{q}\cdot\mathbf{r})|\psi_{n_a\kappa_a m_a}\rangle|^2. \tag{40}$$

Because of the spherical symmetry of closed shells, both the GOS and the TGOS are functions of only the energy loss W and the recoil energy Q (i.e., they depend only on the magnitude of the vector $\mathbf{q}$).

The numerical and kinematical factors in the definitions (39) and (40) are such that, in the limit $Q \to 0$, the longitudinal and transverse GOSs reduce to the familiar optical oscillator strength. The equality of the GOS and the TGOS at $Q = 0$ can be easily proved using the orthogonality of the spherical waves and the relation $\tilde{\boldsymbol{\alpha}} = i(c\hbar)^{-1}[\mathcal{H}_D, \mathbf{r}]$. For recoil energies Q much larger than the ionization energy U, both the GOS and the TGOS differ from zero only in the vicinity of the Bethe ridge ($Q \sim W$). This feature can be evidenced by considering the limiting case of collisions with a free electron at rest, as done by Fano [33]. For this purpose, continuous plane waves of the type (14) can still be used to represent projectile states. However, the initial and final states of the target electron need to be described as discrete plane waves satisfying periodic boundary conditions on a cubic box of unit volume,

$$\varphi_{\mathbf{k}, m_S, +1}(\mathbf{r}) = e^{i\mathbf{k}\cdot\mathbf{r}}U_{\mathbf{k}, m_S, +1}, \tag{41}$$

with wave numbers $\mathbf{k}_a = \mathbf{0}$ and $\mathbf{k}_b$, respectively. The DCS obtained from Fermi's golden rule is

$$\frac{d\sigma^{(\mathrm{FE})}}{d\hat{\mathbf{k}}'} = \frac{(2\pi)^4}{\hbar v}k'\frac{E - W + m_e c^2}{c^2\hbar^2}\sum_{\mathbf{k}_b}\mathcal{T}_2^{(\mathrm{FE})}, \tag{42}$$

where $\mathcal{T}_2^{(\mathrm{FE})}$ is the effective T-matrix element for collisions with free electrons (FE) at rest, including the appropriate sum and averaging over spin states,

$$\mathcal{T}_2^{(\mathrm{FE})} \equiv \frac{1}{4}\sum_{m_{Sa},m_{Sb}}\sum_{m_S,m_{S'}} |\langle \phi_{\mathbf{k}',m_{S'},+1}(0)\varphi_{\mathbf{k}_b,m_{Sb},+1}(1)|\mathcal{H}_{\mathrm{int}}(0,1)|\phi_{\mathbf{k},m_S,+1}(0)\varphi_{0,m_{Sa},+1}(1)\rangle|^2. \tag{43}$$

By following the same steps as in the derivation above, we obtain

$$\frac{d\sigma^{(\mathrm{FE})}}{dQ\,dW} = \frac{2\pi Z_0^2 e^4}{m_e v^2}\left\{\frac{2m_e c^2}{WQ(Q+2m_e c^2)}\left(\frac{(2E-W+2m_e c^2)^2 - Q(Q+2m_e c^2)}{4(E+m_e c^2)^2}\right)\right.$$
$$\left. + \frac{2m_e c^2 W}{[Q(Q+2m_e c^2)-W^2]^2}\left[\beta^2 \sin^2\theta_r + \left(\frac{Q(Q+2m_e c^2)-W^2}{2(E+m_e c^2)^2}\right)\right]\right\}\delta(Q-W). \tag{44}$$

Integration over Q leads to the following energy-loss DCS:

$$\frac{d\sigma^{(\mathrm{FE})}}{dW} = \left(\frac{2\pi Z_0^2 e^4}{m_e v^2}\frac{1}{W^2}\right)F_{\mathrm{rel}}(W), \tag{45}$$

with

$$F_{\mathrm{rel}}(W) = 1 - \frac{(2E-W+4m_e c^2)W}{2(E+m_e c^2)^2}. \tag{46}$$

The energy-loss DCS (45) coincides with the result obtained from elementary quantum electrodynamics for collisions of two distinguishable electrons (see, e.g., [12,48]). In expression (45), the quantity in parentheses is the nonrelativistic (Rutherford) energy-loss DCS and, hence, the factor $F_{\mathrm{rel}}(W)$ accounts for relativistic corrections.

Note that the expression (44) can be expressed in the form (38) with the GOS and the TGOS given by

$$\frac{df^{(\mathrm{FE})}(Q,W)}{dW} = \delta(Q-W) \quad \text{and} \quad \frac{dg^{(\mathrm{FE})}(Q,W)}{dW} = \delta(Q-W), \tag{47}$$

respectively. It is thus clear that, with the definitions (39) and (40), in the high-Q limit the GOS and the TGOS satisfy the Bethe sum rule,

$$\int_0^\infty \frac{df_{n_a\kappa_a}(Q,W)}{dW}dW = 2|\kappa_a|, \quad \int_0^\infty \frac{dg_{n_a\kappa_a}(Q,W)}{dW}dW = 2|\kappa_a|, \tag{48}$$

where $2|\kappa_a|$ is the number of electrons in the active *closed* shell. In the nonrelativistic PWBA, Bethe [49] proved that the total GOS of atoms and positive ions resulting from an independent-electron approximation (including one-electron transitions from any occupied shell to all possible final states, bound and free) satisfies for any Q a sum rule analogous to Eqs. (48), with $2|\kappa_a|$ replaced by the total number of electrons in the atom or ion. In the relativistic case, perturbative calculations [50,51] indicate that deviations from the Bethe sum rule are smaller than about 0.1%, and increase with the atomic number and decrease with Q. Our GOSs satisfy the sum rule (48) only for large values of Q, where the contribution of excitations to final bound states is negligible.

As indicated above, our derivation is similar to that of Fano [33], who explicitly assumed that the mass of the projectile is much larger than the electron mass. The effect of this assumption is simply to remove the quantities in large parentheses on the right-hand side of Eq. (38).

A. Calculation of the GOS and the TGOS

To evaluate the longitudinal GOS, Eq. (39), we introduce the Rayleigh expansion of a plane wave,

$$\exp(i\mathbf{q}\cdot\mathbf{r}) = \sum_{\lambda=0}^{\infty}\sum_{\mu=-\lambda}^{\lambda} i^\lambda(2\lambda+1)j_\lambda(qr)C_{\lambda\mu}(\hat{\mathbf{r}})C^*_{\lambda\mu}(\hat{\mathbf{q}}), \tag{49}$$

where $C_{\lambda\mu}(\hat{\mathbf{r}})=[4\pi/(2\lambda+1)]^{1/2}Y_{\lambda\mu}(\hat{\mathbf{r}})$ are Racah functions. The angular integrals and the summation over magnetic quantum numbers in expression (39) are calculated using elementary angular momentum algebra (see, e.g., Ref. [52]). The result is

$$\frac{df_{n_a\kappa_a}(Q,W)}{dW} = \frac{W2(Q+m_e c^2)}{Q(Q+2m_e c^2)}\sum_{\kappa_b}\frac{k_b}{(\epsilon_{n_a\kappa_a}+W)\pi}(2\lambda+1)$$
$$\times\sum_\lambda \left\langle \ell_a \tfrac{1}{2} j_a\|\mathbf{C}^{(\lambda)}\|\ell_b \tfrac{1}{2} j_b\right\rangle^2 [R^\lambda_{\epsilon_b\kappa_b;n_a\kappa_a}(q)]^2 \tag{50}$$

with the radial integrals

$$R^\lambda_{\epsilon_b\kappa_b;n_a\kappa_a}(q) = \int_0^\infty [P_{\epsilon_b\kappa_b}(r)P_{n_a\kappa_a}(r) + Q_{\epsilon_b\kappa_b}(r)Q_{n_a\kappa_a}(r)]j_\lambda(qr)dr, \tag{51}$$

where $P_{n_a\kappa_a}, Q_{n_a\kappa_a}$ ($P_{\epsilon_b\kappa_b}, Q_{\epsilon_b\kappa_b}$) are the radial functions of the initial (final) orbital of the target electron, which are solutions of the radial Dirac equations (A11). The quantities

$$\left\langle \ell_a \tfrac{1}{2} j_a\|\mathbf{C}^{(\lambda)}\|\ell_b \tfrac{1}{2} j_b\right\rangle = \upsilon(\lambda,\ell_a,\ell_b)(2j_b+1)\left\langle \lambda j_b 0\tfrac{1}{2}|j_a\tfrac{1}{2}\right\rangle^2 \tag{52}$$

are the reduced matrix elements of the Racah tensors in the coupled representation, i.e., in the basis of the spherical spinors $\Omega_{\kappa m}(\hat{\mathbf{r}})$, Eq. (A12). The factor

$$\upsilon(\lambda,\ell_a,\ell_b) = \begin{cases} 1 & \text{if } \lambda+\ell_a+\ell_b \text{ is even,} \\ 0 & \text{otherwise,} \end{cases} \tag{53}$$

accounts for the parity selection rule.

Incidentally, we can now obtain the optical oscillator strength as the $Q \to 0$ limit of the GOS. Using the expansions of the spherical Bessel functions for small arguments (see Ref. [53]), we have

$$\lim_{q\to 0} R^{\lambda}_{\epsilon_b\kappa_b;n_a\kappa_a}(q) = \frac{q^{\lambda}}{(2\lambda+1)!!}\int_0^{\infty} [P_{\epsilon_b\kappa_b}(r)P_{n_a\kappa_a}(r) + Q_{\epsilon_b\kappa_b}(r)Q_{n_a\kappa_a}(r)]r^{\lambda}dr. \tag{54}$$

Because of the orthogonality of the initial and final orbitals, these integrals vanish for $\lambda=0$. The lowest-order nonvanishing contributions are from the dipole terms ($\lambda=1$) and give

$$\frac{df_{n_a\kappa_a}(0,W)}{dW} = \frac{W2m_e}{3\hbar^2}\sum_{\kappa_b}\frac{k_b}{(\epsilon_{n_a\kappa_a}+W)\pi} \times \left\langle \ell_a \tfrac{1}{2} j_a \| \mathbf{C}^{(1)} \| \ell_b \tfrac{1}{2} j_b \right\rangle^2 (\mathcal{D}_{\epsilon_b\kappa_b;n_a\kappa_a})^2, \tag{55}$$

with

$$\mathcal{D}_{\epsilon_b\kappa_b;n_a\kappa_a} = \int_0^{\infty} [P_{\epsilon_b\kappa_b}(r)P_{n_a\kappa_a}(r) + Q_{\epsilon_b\kappa_b}(r)Q_{n_a\kappa_a}(r)]r\,dr. \tag{56}$$

The transverse GOS, Eq. (40), can be evaluated by a method similar to the one adopted by Mann and Johnson [54] for a related integral. We consider a reference frame with the z axis in the direction of the momentum transfer $\mathbf{q}$ (Fig. 1). Rayleigh's expansion (49) then simplifies to

$$\exp(i\mathbf{q}\cdot\mathbf{r}) = \sum_{\lambda} i^{\lambda}[\lambda] j_{\lambda}(qr) C_{\lambda 0}(\hat{\mathbf{r}}), \tag{57}$$

where $[\lambda] \equiv 2\lambda+1$, and the vector $\mathbf{D}$, given by Eq. (25), can be written in the form

$$\mathbf{D} = \sum_{\lambda} i^{\lambda}[\lambda] \langle \psi_{\epsilon_b\kappa_b m_b} | \tilde{\boldsymbol{\alpha}} j_{\lambda}(qr) C_{\lambda 0}(\hat{\mathbf{r}}) | \psi_{n_a\kappa_a m_a} \rangle. \tag{58}$$

Now, it is useful to consider the following identity:

$$\Omega^{\dagger}_{\kappa' m'}(\hat{\mathbf{r}})\boldsymbol{\sigma}\Omega_{\kappa m}(\hat{\mathbf{r}}) = \sum_{J,M}\left[\sqrt{\frac{J}{4\pi}}\left(\frac{\kappa+\kappa'}{J}-1\right)d^J(-\kappa,m;\kappa',m')\mathbf{Y}^{J-1}_{J,M}(\hat{\mathbf{r}}) - \sqrt{\frac{2J+1}{4\pi J(J+1)}}(\kappa-\kappa')d^J(\kappa,m;\kappa',m')\mathbf{Y}^{J}_{J,M}(\hat{\mathbf{r}}) + \sqrt{\frac{J+1}{4\pi}}\left(\frac{\kappa+\kappa'}{J+1}+1\right)d^J(-\kappa,m;\kappa',m')\mathbf{Y}^{J+1}_{J,M}(\hat{\mathbf{r}})\right], \tag{59}$$

where $\mathbf{Y}^{L}_{J,M}(\hat{\mathbf{r}})$ are the vector spherical harmonics (Ref. [55]) and the coefficients $d^J(\kappa,m;\kappa',m')$ are given by

$$d^J(\kappa,m;\kappa',m') = \langle \Omega_{\kappa m} | C_{J,M=m-m'} | \Omega_{\kappa' m'} \rangle = \upsilon(J,\ell,\ell')(-1)^{-m-1/2}\sqrt{[j,j']}\begin{pmatrix} j' & J & j \\ m' & M & -m \end{pmatrix}\begin{pmatrix} j & j' & J \\ \frac{1}{2} & -\frac{1}{2} & 0 \end{pmatrix}, \tag{60}$$

where $[j,j'] \equiv (2j+1)(2j'+1)$ and the notation $(:::)$ denotes Wigner's $3j$ symbols. These d coefficients are the same as those introduced by Grant [56], except for the fact that ours include the parity factor $\upsilon(J,\ell,\ell')$, Eq. (53).

Expressing the central-field orbitals in the form given by Eq. (A10), and using the definition (A12), from Eq. (58) we obtain

$$\mathbf{D} = \sqrt{4\pi}\sum_{\lambda}\sum_{L,J,M} i^{\lambda+1}\sqrt{[\lambda]}C^{L}_{J,M}\int d\hat{\mathbf{r}} Y_{\lambda,0}(\hat{\mathbf{r}})\mathbf{Y}^{L}_{J,M}(\hat{\mathbf{r}}), \tag{61}$$

where the quantities $C^{L}_{J,M}$ are given by

$$C^{J-1}_{J,M} = d^J(\kappa_a,m_a;\kappa_b,m_b)\sqrt{J} \times \int_0^{\infty} dr\left(\frac{\kappa_b-\kappa_a}{J}V^{J-1}_{\epsilon_b\kappa_b;n_a\kappa_a} + U^{J-1}_{\epsilon_b\kappa_b;n_a\kappa_a}\right), \tag{62}$$

$$C^{J}_{J,M} = d^J(-\kappa_a,m_a;\kappa_b,m_b)\sqrt{\frac{2J+1}{J(J+1)}} \times (\kappa_a+\kappa_b)\int_0^{\infty} dr\, V^{J}_{\epsilon_b\kappa_b;n_a\kappa_a}, \tag{63}$$

$$C^{J+1}_{J,M} = d^J(\kappa_a,m_a;\kappa_b,m_b)\sqrt{J+1} \times \int_0^{\infty} dr\left(\frac{\kappa_b-\kappa_a}{J+1}V^{J+1}_{\epsilon_b\kappa_b;n_a\kappa_a} - U^{J+1}_{\epsilon_b\kappa_b;n_a\kappa_a}\right), \tag{64}$$

with

$$V^{\lambda}_{\epsilon_b\kappa_b;n_a\kappa_a} = [P_{\epsilon_b\kappa_b}(r)Q_{n_a\kappa_a}(r) + Q_{\epsilon_b\kappa_b}(r)P_{n_a\kappa_a}(r)]j_{\lambda}(qr), \tag{65}$$

$$U^{\lambda}_{\epsilon_b\kappa_b;n_a\kappa_a} = [P_{\epsilon_b\kappa_b}(r)Q_{n_a\kappa_a}(r) - Q_{\epsilon_b\kappa_b}(r)P_{n_a\kappa_a}(r)]j_{\lambda}(qr). \tag{66}$$

The angular integral in Eq. (61) can be readily evaluated from the definition of the vector spherical harmonics and the

orthogonality property of the spherical harmonics. We obtain

$$\mathbf{D} = \sum_{L,J,M} \sum_{\nu=-1}^{1} (-1)^{L-1+M} i^{\lambda+1} \sqrt{[J,\lambda]} C^{L}_{J,M} \times \begin{pmatrix} L & 1 & J \\ M+\nu & -\nu & -M \end{pmatrix} \delta_{0,M+\nu} \hat{\mathbf{e}}_{-\nu}, \quad (67)$$

where $\hat{\mathbf{e}}_\nu$ are the spherical unit vectors (see Ref. [52]). Replacing the $3j$ coefficient by its analytical expression [52], after some simple but tedious manipulations, we obtain the following expansions for the spherical components of $\mathbf{D}$, $D_{\pm 1} \equiv \mp 2^{-1/2}(D_x \pm i D_y)$:

$$D_{\pm 1} = \sum_{J,M} (-1)^{J+M} i^{J} \left(\frac{(2J+1)^2}{2J(J+1)} \right)^{-1/2} \times [d^J(\kappa_a, m_a; \kappa_b m_b)^{e}\mathcal{R}^{J}_{\epsilon_b \kappa_b; n_a \kappa_a} \pm i d^J(-\kappa_a, m_a; \kappa_b, m_b)^{m}\mathcal{R}^{J}_{\epsilon_b \kappa_b; n_a \kappa_a}] \delta_{0,M\pm 1}, \quad (68)$$

where we have introduced the radial integrals

$${}^{e}\mathcal{R}^{J}_{\epsilon_b \kappa_b; n_a \kappa_a} = \int_0^\infty dr \left(\frac{-J(J+1)}{2J+1} (U^{J-1}_{\epsilon_b \kappa_b; n_a \kappa_a} + U^{J+1}_{\epsilon_b \kappa_b; n_a \kappa_a}) + \frac{(\kappa_b - \kappa_a)}{2J+1} [J V^{J+1}_{\epsilon_b \kappa_b; n_a \kappa_a} - (J+1) V^{J-1}_{\epsilon_b \kappa_b; n_a \kappa_a}] \right) \quad (69)$$

and

$${}^{m}\mathcal{R}^{J}_{\epsilon_b \kappa_b; n_a \kappa_a} = (\kappa_a + \kappa_b) \int_0^\infty dr\, V^{J}_{\epsilon_b \kappa_b; n_a \kappa_a}. \quad (70)$$

The superscripts e and m stand for "electric" and "magnetic," respectively, because these integrals also arise in an alternative treatment based on the multipole expansion of the radiation field (see Ref. [12]).

Using the result given by Eq. (68), together with the relation

$$(2j_a+1) \sum_{m_b} [d^J(\kappa_a, m_a; \kappa_b, m_b)]^2 = \left\langle \ell_a \tfrac{1}{2} j_a \| \mathbf{C}^{(J)} \| \ell_b \tfrac{1}{2} j_b \right\rangle^2, \quad (71)$$

the right-hand side of Eq. (40) can finally be expressed as

$$\frac{dg_{n_a\kappa_a}(Q,W)}{dW} = \frac{2(Q+m_e c^2)}{W} \sum_{\kappa_b} \frac{k_b}{(\epsilon_{n_a\kappa_a} + W)\pi} \sum_{J=1}^{j_a+j_b} \frac{2J+1}{2J(J+1)} \times \left\{ \left[\left\langle \ell_a \tfrac{1}{2} j_a \| \mathbf{C}^{(J)} \| \ell_b \tfrac{1}{2} j_b \right\rangle {}^{e}\mathcal{R}^{J}_{\epsilon_b \kappa_b; n_a \kappa_a}(q) \right]^2 + \left[\left\langle \bar{\ell}_a \tfrac{1}{2} j_a \| \mathbf{C}^{(J)} \| \ell_b \tfrac{1}{2} j_b \right\rangle {}^{m}\mathcal{R}^{J}_{\epsilon_b \kappa_b; n_a \kappa_a}(q) \right]^2 \right\}, \quad (72)$$

where the quantum number $\bar{\ell}_a$ is defined by Eq. (A25).

A FORTRAN code, originally developed by Segui *et al.* [30] to compute the GOS for ionization of inner shells of atoms and positive ions, has been improved and extended to include the calculation of the TGOS. As in the original code, radial Dirac functions are calculated using the subroutine package RADIAL [57], which implements a numerical algorithm that effectively avoids the accumulation of truncation errors. From a comparison with analytical nonrelativistic hydrogenic GOSs, Segui *et al.* estimated that the GOSs given by the original code were accurate to five significant digits. A similar analysis indicates that our extended code is slightly more accurate.

Our code calculates the GOS and the TGOS for a grid of discrete values of the reduced variables $t \equiv Q/U$ and $w \equiv (W/U) - 1$, from which the values of the GOSs at arbitrary points (t,w) are evaluated by using suitable interpolation-extrapolation schemes. The w grid is logarithmic and extends from 10^{-5} up to a value $w_{\max}$, of the order of 100, where the convergence of the numerical series starts deteriorating. The t grid, which is determined independently for each value of w, spans the interval from 10^{-6} up to a value $\sim 1.5 w_{\max}$, where the GOS and the TGOS take values of the order of 10^{-7}. For larger t values, both functions decrease rapidly with t, roughly as t^{-n} with n between 3 and 7. For a given w, the points of the t grid are unevenly distributed, with the higher concentration in regions where the tabulated function varies more rapidly, to allow accurate linear log-log interpolation in t. Examples of calculated GOSs for the K $(1s_{1/2})$ shell of Ar and the $M1$ $(3s_{1/2})$ shell of Cu are shown in Fig. 2.

The GOSs can be represented as a surface on the (Q,W) plane, the so-called Bethe surface [34]. As illustrated in Fig. 2, for each value of w the GOS has a prominent maximum at $t \sim w$, the Bethe ridge [34], which corresponds to collisions with relatively large momentum transfers (close collisions). When w increases, the position of the Bethe ridge shifts to larger t values. Hence, near the Bethe ridge the GOS varies rapidly along the directions of both the w and the t axes. To devise an efficient interpolation scheme, it is advantageous to introduce a transformation that renders the position of the GOS maximum nearly constant with w, thus reducing the fast variation of the GOS with w. Previous work on the relationship between the PWBA and the impulse approximation [58] indicates that the transformation from the GOS to the W-dependent Born-Compton profile meets our needs. The longitudinal (L) and transverse (T) Born-Compton profiles, defined by Eq. (55) of Ref. [58], are

$$J^{\mathrm{L}}_{n_a\kappa_a}(W; p_{\mathrm{C}}) = \frac{c\sqrt{Q(Q+2m_e c^2)}}{(Q+m_e c^2)} \frac{Q(1+Q/2m_e c^2)}{W(1+W/2m_e c^2)} \frac{df_{n_a\kappa_a}(Q,W)}{dW} \quad (73a)$$

and

$$J^{\mathrm{T}}_{n_a\kappa_a}(W; p_{\mathrm{C}}) = \frac{c\sqrt{Q(Q+2m_e c^2)}}{(Q+m_e c^2)} \frac{Q(1+Q/2m_e c^2)}{W(1+W/2m_e c^2)} \frac{dg_{n_a\kappa_a}(Q,W)}{dW}, \quad (73b)$$

respectively. The variable p_{C}, which in the impulse approximation represents the minimum momentum of the target electron for which the kinematical constraints imposed by

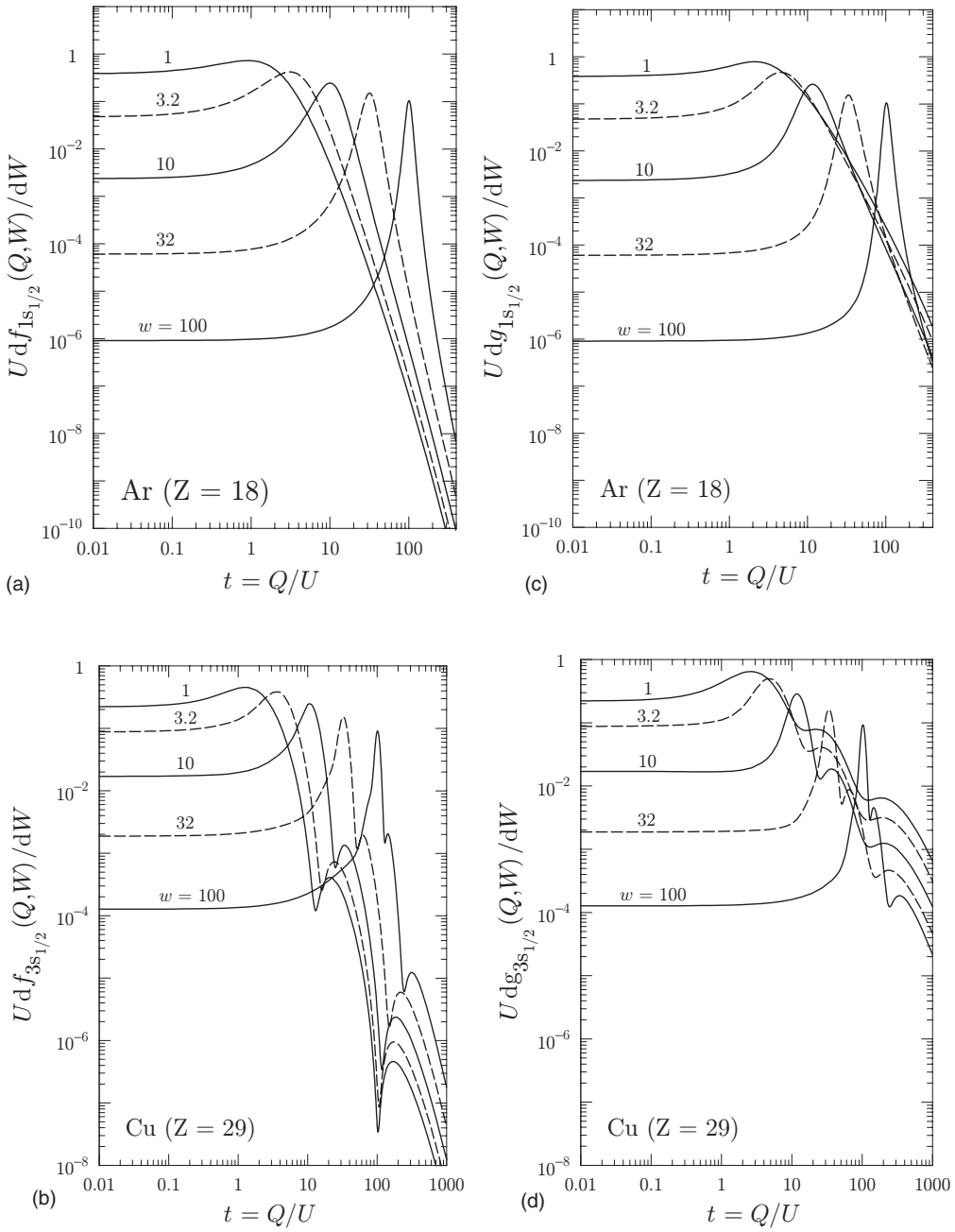

FIG. 2. Longitudinal (left) and transverse (right) GOSs of the K shell of Ar and for the $M1$ shell of Cu, in atomic units (a.u.). Each curve represents the GOS for the indicated value of $w=(W/U)-1$ as a function of $t=Q/U$.

momentum and energy conservation are satisfied, is defined as

$$p_C = -\frac{1}{2c}\left(\sqrt{Q(Q+2m_ec^2)} - W\sqrt{1+\frac{(2m_ec^2)^2}{Q(Q+2m_ec^2)-W^2}}\right) \quad \text{if } W \le Q \tag{74a}$$

and

$$p_C = \frac{2(Q+m_ec^2)(W-Q)}{2c\sqrt{Q(Q+2m_ec^2)}} + \frac{[3m_ec^2(Q+m_ec^2)+Q^2](W-Q)^2}{2c\sqrt{Q(Q+2m_ec^2)}(Q+2m_ec^2)m_ec^2} \quad \text{if } W > Q. \tag{74b}$$

The Born-Compton profiles obtained from the GOSs of Fig. 2 are displayed in Fig. 3. The smooth variation of these profiles with w is evident (cf. Figs. 2 and 3). In our computer code, the GOSs and the TGOSs are replaced by the corresponding Born-Compton profiles. To compute the GOSs at a

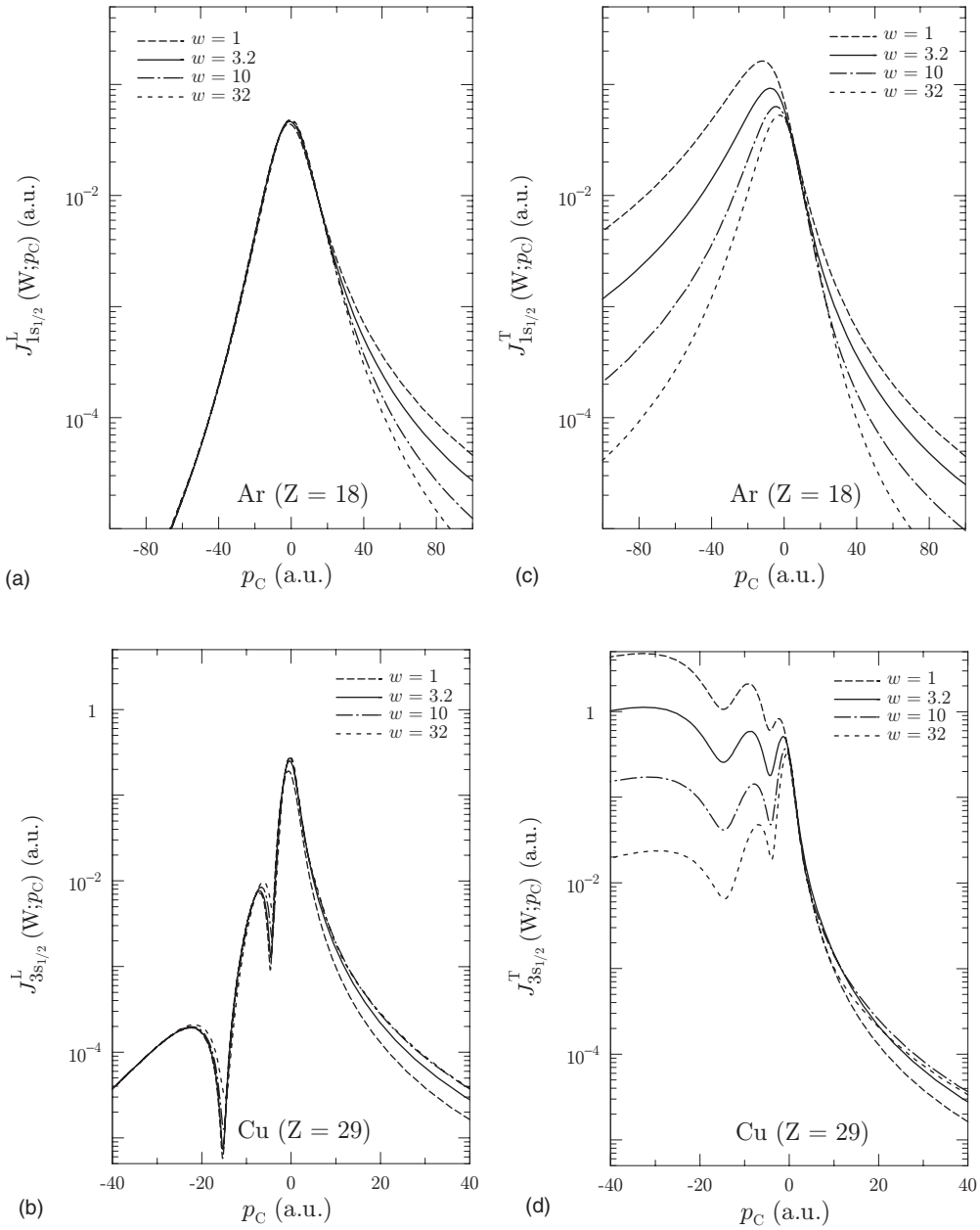

FIG. 3. Longitudinal (L) and transverse (T) Born-Compton profiles, Eqs. (73a) and (73b), of the K shell of Ar and of the $M1$ shell of Cu, in atomic units. Each curve represents the profiles for the indicated value of $w=(W/U)-1$ as a function of the variable p_C, Eqs. (74a) and (74b).

given point (Q,W), we use linear log-log interpolation of the Born-Compton profiles in both $t=Q/U$ and $w=(W/U)-1$, and obtain the GOSs by inverting the transformations (73a) and (73b). The numerical error introduced by these interpolations is estimated to cause variations in the calculated total ionization cross sections that are less than 0.1%.

For a given energy loss W, the allowed recoil energies are limited to the interval (Q_-,Q_+) with (see, e.g., Ref. [58])

$$Q_\pm = \sqrt{(cp \pm cp')^2 + m_e^2c^4} - m_ec^2$$
$$= \sqrt{\left[\sqrt{E(E+2mc^2)} \pm \sqrt{(E-W)(E-W+2mc^2)}\right]^2 + m_e^2c^4} - m_ec^2. \quad (75)$$

The energy-loss DCS is obtained by integrating the DDCS over the recoil energy,

$$\frac{d\sigma^{(\mathrm{PW})}}{dW} = \int_{Q_-}^{Q_+} \frac{d\sigma^{(\mathrm{PW})}}{dW\,dQ} dQ. \quad (76)$$

A further integration over W yields the total ionization cross section,

$$\sigma^{(\mathrm{PW})} = \int_U^E \frac{d\sigma^{(\mathrm{PW})}}{dW} dW. \quad (77)$$

For energy transfers W larger than the upper limit of the numerical GOS tables, $(w_{\max}+1)U$, the energy-loss DCS is

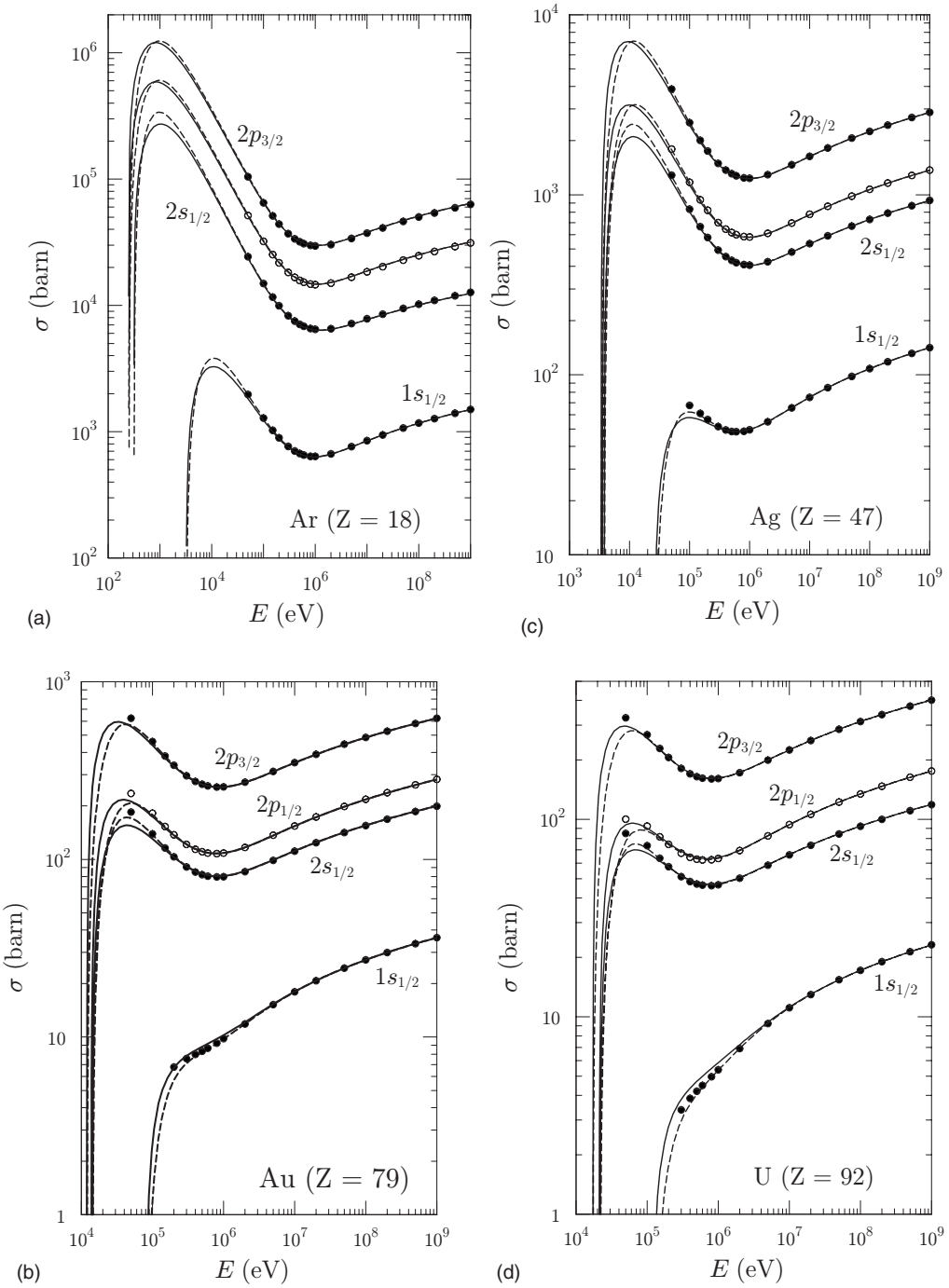

FIG. 4. Calculated total electron-impact ionization cross sections for the K shell and the L subshells of the indicated elements obtained from the present PWBA Eq. (77) (dashed lines) and from the corrected PWBA Eq. (99) (solid lines). Circles represent PWBA results from Scofield [12].

approximated by the free-electron DCS, Eq. (45). Our approach is thus completely equivalent to the one adopted by Scofield [12]. Calculated total cross sections for K and L shells of the elements Ar, Ag, Au, and U are compared with results from Scofield's calculation in Fig. 4. Differences are visible only for the lowest energies considered by Scofield, and they are probably due to the different interpolation schemes used to evaluate the DDCSs.

It should be noted that in the derivation of the PWBA cross sections we have been ignoring electron exchange effects. Exchange effects occur also in the case of positron collisions, because of the indistinguishability of the initial electron from the virtual electrons in states of negative energy. In the energy range where the PWBA is expected to be reliable, the total cross section is known to be fairly insensitive to these effects. However, electron exchange introduces appreciable modifications in the stopping power and the energy straggling of both electrons and positrons. It is difficult to make allowance for exchange within the PWBA, mainly because the projectile plane waves are not orthogonal to the

bound and free orbitals of the active electron. Exchange corrections can be calculated consistently only in the case of collisions with free electrons at rest (because both the projectile and the target are then described by plane waves). The corresponding exchange-corrected PWBA DCSs for projectile electrons and positrons are given by simple analytical formulas, which were derived by Møller [59] and Bhabha [60], respectively. The common approach adopted to account for the effect of electron exchange on the stopping power of electrons and positrons is based on the fact that, for energy transfers W much larger than the ionization energy U, the target electron can be regarded as free. The well-known Bethe-Bloch formula for the stopping power [32,61,62] is obtained by assuming that the energy-loss DCS for large-W collisions can be approximated by the Møller or Bhabha formulas.

IV. DISTORTED-WAVE BORN APPROXIMATION

As indicated above, the present calculations are based on the DWBA as formulated by Segui *et al.* [30]. For the sake of completeness, we summarize here the basic assumptions and the resulting formulas for the energy-loss DCS, in a slightly modified form that is better suited to our present purposes. The initial and final orbitals of the active target electron are Dirac central-field orbitals for the potential $V_{\mathrm{T}}(r)=V^{(\mathrm{DFS})}(r)$, while the distorted plane waves of the projectile are calculated with the potential $V_{\mathrm{P}}(r)$ given by Eq. (5), which in the case of electrons is the same as the potential experienced by the target electron. The interaction between the projectile and the active electron is assumed to be purely Coulombian,

$$\mathcal{H}_{\mathrm{int}}^{\mathrm{L}}(0,1)=-\frac{Z_0e^2}{|\mathbf{r}-\mathbf{r}_0|}. \tag{78}$$

Although we use relativistic wave functions, this form of the DWBA can be qualified as semirelativistic only, because the effect of the transverse interaction is disregarded.

Expanding the Coulomb potential in terms of spherical Racah tensors [52],

$$\frac{1}{|\mathbf{r}_0-\mathbf{r}|}=\sum_{L=0}^{\infty}\frac{r_<^L}{r_>^{L+1}}\mathbf{C}^{(L)}(\hat{\mathbf{r}}_0)\cdot\mathbf{C}^{(L)}(\hat{\mathbf{r}}), \tag{79}$$

with $r_<=\min(r_0,r)$ and $r_>=\max(r_0,r)$, the sums and averages over degenerate states in Eq. (11), as well as the angular integral in Eq. (13), can be readily evaluated using elementary angular momentum algebra. The resulting energy-loss DCS for positrons can be expressed as

$$\frac{d\sigma_+^{(\mathrm{DW,L})}}{dW}=\frac{2Z_0^2e^4}{\hbar v}\frac{(E-W+2m_ec^2)(W-U+2m_ec^2)}{c^4\hbar^4k^2k'k_b}\times\frac{E+2m_ec^2}{E+m_ec^2}\sum_{\kappa_b}\sum_{\kappa}\sum_{\kappa'}\sum_{L}\frac{1}{[L]}(X^{\epsilon\kappa;n_a\kappa_a}_{\epsilon'\kappa';\epsilon_b\kappa_b;L})^2, \tag{80}$$

where

$$X^{\epsilon\kappa;n_a\kappa_a}_{\epsilon'\kappa';\epsilon_b\kappa_b;L}\equiv\langle\ell_a\tfrac{1}{2}j_a\|\mathbf{C}^{(L)}\|\ell_b\tfrac{1}{2}j_b\rangle\times\langle\ell\tfrac{1}{2}j\|\mathbf{C}^{(L)}\|\ell'\tfrac{1}{2}j'\rangle R^{\epsilon\kappa;n_a\kappa_a}_{\epsilon'\kappa';\epsilon_b\kappa_b;L}, \tag{81}$$

and the quantities $R^{\epsilon\kappa;n_a\kappa_a}_{\epsilon'\kappa';\epsilon_b\kappa_b;L}$ are Slater integrals,

$$R^{\epsilon\kappa;n_a\kappa_a}_{\epsilon'\kappa';\epsilon_b\kappa_b;L}=\iint dr_0dr\frac{r_<^L}{r_>^{L+1}}\times[P_{\epsilon\kappa}(r_0)P_{\epsilon'\kappa'}(r_0)+Q_{\epsilon\kappa}(r_0)Q_{\epsilon'\kappa'}(r_0)]\times[P_{n_a\kappa_a}(r)P_{\epsilon_b\kappa_b}(r)+Q_{n_a\kappa_a}(r)Q_{\epsilon_b\kappa_b}(r)]. \tag{82}$$

In the case of projectile electrons, exchange effects are accounted for by antisymmetrizing the initial and final states. Since the target and projectile electrons are assumed to move under the same (DFS) potential, their orbitals are orthogonal, and the transition matrix element takes the form

$$T^{(\mathrm{s})}_{ba,-}\equiv\langle\psi^{(-)}_{\mathbf{k}'m_{\mathrm{S}}'}(0)\psi_{\epsilon_b\kappa_bm_b}(1)|\mathcal{H}^{\mathrm{L}}_{\mathrm{int}}(0,1)|\psi^{(+)}_{\mathbf{k}m_{\mathrm{S}}}(0)\psi_{n_a\kappa_am_a}(1)\rangle-\langle\psi^{(-)}_{\mathbf{k}'m_{\mathrm{S}}'}(1)\psi_{\epsilon_b\kappa_bm_b}(0)|\mathcal{H}^{\mathrm{L}}_{\mathrm{int}}(0,1)|\psi^{(+)}_{\mathbf{k}m_{\mathrm{S}}}(0)\psi_{n_a\kappa_am_a}(1)\rangle. \tag{83}$$

The energy-loss DCS for electrons is obtained by following the same steps as for positrons, and is

$$\frac{d\sigma_-^{\mathrm{DW,L}}}{dW}=\frac{2Z_0^2e^4}{\hbar v}\frac{(E-W+2m_ec^2)(W-U+2m_ec^2)}{c^4\hbar^4k^2k'k_b}\times\frac{E+2m_ec^2}{E+m_ec^2}\sum_{\kappa}\sum_{\kappa'}\sum_{\kappa_b}\times\left(\sum_L\frac{1}{[L]}(X^{\epsilon\kappa;n_a\kappa_a}_{\epsilon'\kappa';\epsilon_b\kappa_b;L})^2+\sum_{L'}\frac{1}{[L']}(X^{\epsilon\kappa;n_a\kappa_a}_{\epsilon_b\kappa_b;\epsilon'\kappa';L'})^2-2\sum_L\sum_{L'}(-1)^{L+L'+1}\begin{Bmatrix}j_a & j_b & L\\ j & j' & L'\end{Bmatrix}\times X^{\epsilon\kappa;n_a\kappa_a}_{\epsilon'\kappa';\epsilon_b\kappa_b;L}X^{\epsilon\kappa;n_a\kappa_a}_{\epsilon_b\kappa_b;\epsilon'\kappa';L'}\right), \tag{84}$$

where $\{:::\}$ denote Wigner's $6j$ symbols. The coefficient $X^{\epsilon\kappa,n_a\kappa_a}_{\epsilon_b\kappa_b,\epsilon\kappa,L}$ is obtained from (81) by the interchange $\epsilon'\kappa'\leftrightarrow\epsilon_b\kappa_b$ $(E-W\leftrightarrow W-U)$. The first and second terms in the large parentheses correspond to direct and exchange transitions, respectively. The third term results from the interference between the direct and exchange scattered waves. Details on the numerical calculation of the energy-loss DCSs given by Eqs. (80) and (84) can be found in Ref. [30].

It is worth noting that the energies of the two electrons after the interaction are $E-W$ and $W-U$. If, following the usual convention, we consider the "primary" electron as the fastest, the allowed values of the energy loss are such that $W-U\leq E-W$, that is,

$$W \le W_{\max} = \frac{1}{2}(E+U). \tag{85}$$

If the projectile and target electrons were distinguishable, the energy-loss DCS would be given by expression (84) with the second and third terms in the large parentheses removed [cf. Eq. (80)] and, moreover, energy transfers from U to E would be allowed. Indeed, the second term on the right-hand side of Eq. (84) represents collisions where, if the electrons were distinguishable, the projectile would lose an energy W larger than $W_{\max}$. Evidently, in the case of positron collisions, the maximum allowed energy loss is $W_{\max}=E$.

A. Distortion and exchange corrections to the PWBA

The semirelativistic DWBA calculations described in Ref. [30] yield total cross sections in fairly good agreement with experimental data for ionization of K and L shells [63–65]. However, these calculations are feasible only for projectiles with kinetic energies up to about $10U$. On the other hand, the relativistic PWBA cross sections can be easily calculated for arbitrary energies. Moreover, the effect of the transverse interaction, which is ignored in the DWBA, is properly accounted for within the PWBA.

Comparison of total ionization cross sections calculated from the DWBA and from the PWBA can be used to estimate the error introduced by the latter at low energies. To make the comparison meaningful, we temporarily neglect the transverse term in the PWBA cross sections. The calculations reported below indicate that, for $E \gtrsim 10U$, the difference between the total ionization cross sections obtained from the DWBA and the PWBA decreases in magnitude as the energy of the projectile increases and is less than $\sim 5\%$ for E larger than about $20U$. Differences between the corresponding DCSs may be substantial at these energies, but they arise only from partial waves with small and moderate orbital angular momenta ℓ. When ℓ is large, the centrifugal barrier keeps the projectile far from the nucleus, where the distorting potential $V_{\rm P}(r)$ is small, and then the PWBA is expected to provide the correct contribution to the DCS. In other words, the partial-wave series for the difference between the DWBA and the PWBA cross sections may be expected to converge faster than the DWBA series.

As mentioned above, when the distorting potential V_P is reduced to zero, the DPWs reduce to positive-energy plane waves, i.e.,

$$\psi^{(\pm)}_{\mathbf{k}\mu}(\mathbf{r}) \to \phi_{\mathbf{k},\mu,+1}(\mathbf{r}) \quad \text{if} \quad V_P \to 0. \tag{86}$$

Thus, the PWBA T-matrix elements

$$T^{(\rm PWs)}_{ba} = \langle \phi_{\mathbf{k}',m_{S'},+1}(0)\psi_{\epsilon_b\kappa_b m_b}(1)|\mathcal{H}_{\rm int}(0,1) \times |\phi_{\mathbf{k},m_S,+1}(0)\psi_{n_a\kappa_a m_a}(1)\rangle \tag{87}$$

can be considered as the $V_{\rm P}\to 0$ limit of the DWBA T-matrix elements (12). In this limit, the radial functions of the projectile reduce to spherical Bessel functions; see Eq. (A23). Hence, the PWBA energy-loss DCS for positrons (considering only the longitudinal interaction) can be evaluated by using the same formulas as for the DWBA calculation, Eqs. (80) and (84), with the projectile radial functions replaced by Bessel functions. That is,

$$\frac{d\sigma^{\rm PW,L}_{+}}{dW} = \frac{2Z_0^2e^4}{\hbar v}\frac{(E-W+2m_ec^2)(W-U+2m_ec^2)}{c^4\hbar^4k^2k'k_b} \times \frac{E+2m_ec^2}{E+m_ec^2} \times \sum_{\kappa_b}\sum_{\kappa}\sum_{\kappa'}\sum_{L}\frac{1}{[L]}(\tilde{X}^{\epsilon\kappa;n_a\kappa_a}_{\epsilon'\kappa';\epsilon_b\kappa_b;L})^2, \tag{88}$$

with

$$\tilde{X}^{\epsilon\kappa;n_a\kappa_a}_{\epsilon'\kappa';\epsilon_b\kappa_b;L} = \left\langle \ell_a \tfrac{1}{2} j_a \| \mathbf{C}^{(L)} \| \ell_b \tfrac{1}{2} j_b \right\rangle \left\langle \ell \tfrac{1}{2} j \| \mathbf{C}^{(L)} \| \ell' \tfrac{1}{2} j' \right\rangle \tilde{R}^{\epsilon\kappa;n_a\kappa_a}_{\epsilon'\kappa';\epsilon_b\kappa_b;L} \tag{89}$$

and

$$\tilde{R}^{\epsilon\kappa;n_a\kappa_a}_{\epsilon'\kappa';\epsilon_b\kappa_b;L} = \iint dr_0 dr \frac{r_<^L}{r_>^{L+1}} \times [P^{(0)}_{\epsilon\kappa}(r_0)P^{(0)}_{\epsilon'\kappa'}(r_0) + Q^{(0)}_{\epsilon\kappa}(r_0)Q^{(0)}_{\epsilon'\kappa'}(r_0)] \times [P_{n_a\kappa_a}(r)P_{\epsilon_b\kappa_b}(r) + Q_{n_a\kappa_a}(r)Q_{\epsilon_b\kappa_b}(r)], \tag{90}$$

where $P^{(0)}_{\epsilon\kappa}(r)$ and $Q^{(0)}_{\epsilon\kappa}(r)$ are the radial functions for positive-energy free states, given by Eqs. (A23). The difference between the cross sections for positrons obtained from the DWBA and the PWBA can then be expressed as

$$\frac{d\Delta\sigma_+}{dW} \equiv \frac{d\sigma^{\rm (DW,L)}_{+}}{dW} - \frac{d\sigma^{\rm (PW,L)}_{+}}{dW} = \frac{2Z_0^2e^4}{\hbar v}\frac{(E-W+2m_ec^2)(W-U+2m_ec^2)}{c^4\hbar^4k^2k'k_b} \times \frac{E+2m_ec^2}{E+m_ec^2}\sum_{\kappa_b}\sum_{\kappa}\sum_{\kappa'}\sum_{L}\frac{1}{[L]}\Delta X^{\epsilon\kappa;n_a\kappa_a}_{\epsilon'\kappa';\epsilon_b\kappa_b;L} \times (2\tilde{X}^{\epsilon\kappa;n_a\kappa_a}_{\epsilon'\kappa';\epsilon_b\kappa_b;L} + \Delta X^{\epsilon\kappa;n_a\kappa_a}_{\epsilon'\kappa';\epsilon_b\kappa_b;L}), \tag{91}$$

where

$$\Delta X^{\epsilon\kappa;n_a\kappa_a}_{\epsilon'\kappa';\epsilon_b\kappa_b;L} = X^{\epsilon\kappa;n_a\kappa_a}_{\epsilon'\kappa';\epsilon_b\kappa_b;L} - \tilde{X}^{\epsilon\kappa;n_a\kappa_a}_{\epsilon'\kappa';\epsilon_b\kappa_b;L} \tag{92}$$

is the "correction" to the PWBA X coefficient.

Similarly, for electrons we have

$$\frac{d\sigma^{\rm (PW,L)}_{-}}{dW} = \frac{2Z_0^2e^4}{\hbar v}\frac{(E-W+2m_ec^2)(W-U+2m_ec^2)}{c^4\hbar^4k^2k'k_b} \times \frac{E+2m_ec^2}{E+m_ec^2}\sum_{\kappa_b}\sum_{\kappa}\sum_{\kappa'}\left(\sum_{L}\frac{1}{[L]}(\tilde{X}^{\epsilon\kappa,n_a\kappa_a}_{\epsilon'\kappa',\epsilon_b\kappa_b,L})^2 + \sum_{L'}\frac{1}{[L']}(\tilde{X}^{\epsilon\kappa,n_a\kappa_a}_{\epsilon_b\kappa_b,\epsilon'\kappa',L'})^2\right), \tag{93}$$

and the corresponding correction is given by

$$\frac{d\Delta\sigma_-}{dW} \equiv \frac{d\sigma_-^{(\mathrm{DW,L})}}{dW} - \frac{d\sigma_-^{(\mathrm{PW,L})}}{dW} = \frac{2Z_0^2e^4}{\hbar v}\frac{(E-W+2m_ec^2)(W-U+2m_ec^2)}{c^4\hbar^4k^2k'k_b}\frac{E+2m_ec^2}{E+m_ec^2}\sum_{\kappa_b}\sum_{\kappa}\sum_{\kappa'}$$
$$\times\left(\sum_L \frac{1}{[L]}\Delta X^{\epsilon\kappa;n_a\kappa_a}_{\epsilon'\kappa';\epsilon_b\kappa_b;L}(2\tilde{X}^{\epsilon\kappa;n_a\kappa_a}_{\epsilon'\kappa';\epsilon_b\kappa_b;L} + \Delta X^{\epsilon\kappa;n_a\kappa_a}_{\epsilon'\kappa';\epsilon_b\kappa_b;L}) + \sum_{L'}\frac{1}{[L']}\Delta X^{\epsilon\kappa;n_a\kappa_a}_{\epsilon_b\kappa_b;\epsilon'\kappa';L'}(2\tilde{X}^{\epsilon\kappa;n_a\kappa_a}_{\epsilon_b\kappa_b;\epsilon'\kappa';L'} + \Delta X^{\epsilon\kappa;n_a\kappa_a}_{\epsilon_b\kappa_b;\epsilon'\kappa';L'})\right.$$
$$\left. - 2\sum_L\sum_{L'}(-1)^{L+L'+1}\begin{Bmatrix} j_a & j_b & L \\ j & j' & L' \end{Bmatrix} X^{\epsilon\kappa,n_a\kappa_a}_{\epsilon'\kappa',\epsilon_b\kappa_b,L}X^{\epsilon\kappa,n_a\kappa_a}_{\epsilon_b\kappa_b,\epsilon'\kappa',L'}\right). \tag{94}$$

At this point, we can combine the energy-loss DCS obtained from the PWBA defined by Eq. (76), considering only the contribution from the longitudinal interaction, with the DWBA correction given by Eqs. (94) and (91) for electrons and positrons, respectively,

$$\frac{d\sigma_\pm^{(\mathrm{L})}}{dW} = \frac{d\sigma^{(\mathrm{PW,L})}}{dW} + \frac{d\Delta\sigma_\pm}{dW}. \tag{95}$$

Finally, integration of these DCSs over the energy loss yields the total ionization cross section,

$$\sigma_\pm^{(\mathrm{L})} = \int_U^E \frac{d\sigma^{(\mathrm{PW,L})}}{dW}dW + \int_U^{W_{\max}}\frac{d\Delta\sigma_\pm}{dW}dW = \sigma^{(\mathrm{PW,L})} + \Delta\sigma_\pm^{(\mathrm{L})}. \tag{96}$$

Here the maximum energy loss in the PWBA term is set equal to E, for both electrons and positrons, because exchange effects are being disregarded in the PWBA. Notice, however, that in the case of electron collisions the correction $\Delta\sigma_\pm^{(\mathrm{L})}$ does account for exchange effects in a consistent way. We shall refer to the DWBA, calculated as formulated in Eqs. (95) and (96), as the "corrected" PWBA (CPWBA). Note that, for the energies where the partial-wave series do converge, the DCSs and total ionization cross sections calculated using the CPWBA formulas coincide with those resulting from the semirelativistic DWBA.

Numerical calculations show that the expansions (91) and (94) do not converge faster than the corresponding DWBA series, Eqs. (80) and (84). Nevertheless, for large angular momenta, the contribution to the DCS of each term in the expansions (91) and (94) is much smaller than that of the term of (80) and (84) with the same angular momentum. Moreover, the calculation of the longitudinal part of the PWBA, $d\sigma^{(\mathrm{PW,L})}/dW$, is free from convergence problems (at least for the moderately low energies considered here). As a consequence, the calculation of the corrections given by Eqs. (91) and (94) is practically more effective than the straight calculation of the DWBA series. This peculiarity is illustrated in Table I, which shows ratios of total cross sections for ionization of gold atoms by electron impact evaluated from the DWBA and the CPWBA, i.e., from the partial-wave expansions (84) and (94), respectively. In both cases, the summations over κ, κ', and κ_b were truncated at the cutoff value $\kappa_{\max}$ indicated in the table. Note that the results shown in Table I were calculated by using only the longitudinal interaction. We consider the cross section obtained from the corrected PWBA with the highest cutoff, $\kappa_{\max}=30$, as the "exact" cross section. The tabulated quantity is the ratio of each cross section to this exact value. We see that the CPWBA converges more rapidly than the DWBA. The former already approaches the exact value to within 1.5% with $\kappa_{\max}=15$, while the DWBA reaches this degree of accuracy only with $\kappa_{\max}=30$. To keep the calculation time within reasonable limits, all the numerical results reported below were obtained with $\kappa_{\max}=20$ so that truncation errors are probably less than ~0.5%.

V. TOTAL IONIZATION CROSS SECTIONS

To obtain cross sections valid at high energies and for high-Z atoms, we have to account for the effect of the transverse interaction. Since the contribution from this interaction is only appreciable for high-energy projectiles, it will be described by using the PWBA (see Sec. III). The energy-loss DCS, including both the longitudinal and transverse contributions, can thus be expressed as

$$\frac{d\sigma_\pm}{dW} = \frac{d\sigma^{(\mathrm{PW})}}{dW} + \frac{d\Delta\sigma_\pm}{dW}, \tag{97}$$

where the PWBA energy-loss DCS is given by Eq. (76), and

$$\sigma_\pm = \int_U^E \frac{d\sigma^{(\mathrm{PW})}}{dW}dW + \int_U^{W_{\max}}\frac{d\Delta\sigma_\pm}{dW}dW = \sigma^{(\mathrm{PW})} + \Delta\sigma_\pm. \tag{98}$$

With our computer codes, the calculation of the CPWBA cross section given by Eq. (98) can be performed only for kinetic energies E up to about $25U$, partially because the partial-wave series Eqs. (91) and (94) are truncated at $\kappa_{\max}$. The computer time needed to evaluate these series depends on the kinetic energy of the projectile. The calculation is faster for near-threshold energies because the partial-wave series converges with a relatively small number of terms. When the energy increases, the number of terms needed to achieve numerical convergence increases and, consequently, the calculation time also rises. On a Pentium IV 3 MHz processor, calculations of the total ionization cross section Eq. (98) for electrons with $E=1.02U$ and $16U$ take about 10 and 90 min, respectively.

CPWBA ionization cross sections have been calculated for the K shell and the L and M subshells of all elements, from hydrogen ($Z=1$) to einsteinium ($Z=99$), for electrons

TABLE I. Convergence of the DWBA series Eq. (84) and the CPWBA series Eq. (94) for the case of ionization of inner shells of gold atoms by impact of electrons with $E=10U$. The tabulated quantity is the ratio of the total ionization cross sections obtained from the DWBA and from the corrected CPWBA, Eq. (97), with the corresponding partial-wave series truncated at the indicated value of κ_{max}, to the "exact" cross section (CPWBA with $\kappa_{max}=30$).

		κ_{max}				
Shell	Method	10	15	20	25	30
$1s_{1/2}$	DWBA	0.700	0.890	0.961	0.986	0.996
	CPWBA	0.965	0.988	0.996	0.999	1.000
$2s_{1/2}$	DWBA	0.609	0.854	0.946	0.978	0.991
	CPWBA	0.975	0.987	0.996	0.999	1.000
$2p_{1/2}$	DWBA	0.650	0.863	0.945	0.978	0.992
	CPWBA	0.964	0.987	0.996	0.999	1.000
$2p_{3/2}$	DWBA	0.639	0.858	0.941	0.974	0.989
	CPWBA	0.965	0.987	0.996	0.999	1.000
$3s_{1/2}$	DWBA	0.507	0.798	0.926	0.970	0.987
	CPWBA	0.994	0.985	0.995	0.999	1.000
$3p_{1/2}$	DWBA	0.538	0.809	0.924	0.967	0.985
	CPWBA	0.980	0.984	0.995	0.999	1.000
$3p_{3/2}$	DWBA	0.532	0.808	0.923	0.966	0.985
	CPWBA	0.978	0.984	0.995	0.999	1.000
$3d_{3/2}$	DWBA	0.583	0.826	0.924	0.965	0.984
	CPWBA	0.954	0.984	0.995	0.999	1.000
$3d_{5/2}$	DWBA	0.585	0.826	0.924	0.965	0.984
	CPWBA	0.956	0.984	0.995	0.999	1.000

and positrons with kinetic energies E ranging from $1.02U$ ($1.05U$ for positrons) to $16U$. The PWBA Eq. (77) gives total cross sections that at $E=16U$ differ from our CPWBA values by less than about 7%. This difference is mostly due to the neglect of the distortion of the projectile waves by the atomic potential, because the interference term in the DWBA energy-loss DCS, Eq. (84), decreases rapidly with E. Some authors have suggested that the effect of distortion can be approximately accounted for by assuming that a projectile electron acquires an additional kinetic energy bU when it falls within the potential well of the atom (see, e.g., Refs. [19] and [37]). The most visible energy dependence of the PWBA cross section is through the factor $m_e v^2$ in the denominator of Eq. (38), which in the nonrelativistic domain is proportional to the kinetic energy of the projectile. Consequently, we can modify the PWBA empirically by multiplying it by a scaling factor $E/(E+bU)$, where b is an energy-independent parameter characteristic of each element and atomic shell. Thus, the total ionization cross section is obtained as

$$\sigma_{\pm} = \begin{cases} \sigma^{(\mathrm{PW})} + \Delta\sigma_{\pm} & \text{if } E \leq 16U, \\ \dfrac{E}{E+bU}\sigma_{\pm}^{(\mathrm{PW})} & \text{if } E > 16U, \end{cases} \tag{99}$$

where the value of the scaling parameter b is determined by requiring continuity at $E=16U$. Notice that the scaling factor $E/(E+bU)$ tends to unity at high energies ($E \gg U$), i.e., it leaves the PWBA cross section unaltered where it is expected to be reliable.

Figure 5 displays total cross sections obtained from Eq. (99) for ionization of the K and $M2$ ($3p_{1/2}$) shells of uranium atoms by impact of electrons as functions of the kinetic energy. Open circles represent the results from numerical CPWBA calculations Eq. (98); dashed curves represent the PWBA cross section Eq. (77), and the continuous curves are the results from Eq. (99). Note that the two branches of Eq. (99) do match smoothly at the point $E=16U$, which is indicated by the vertical lines. We have also performed sample calculations with the CPWBA Eq. (99), for energies E larger than $16U$, up to about $20U$, and found that the results agree to within about 0.2% with those of the scaled PWBA. It is interesting to note that for K shells of heavy elements the PWBA yields cross sections that are smaller than those from the CPWBA, in the energy interval where the latter can be effectively calculated. This peculiarity is in contradiction to the naive assumption that the PWBA can be partially corrected by assuming that the effect of the atomic potential on the projectile wave functions is equivalent to a net *increase* in kinetic energy [19,37].

VI. COMPARISON WITH EXPERIMENTAL DATA

Measurements of total ionization cross sections have been performed by many groups since the early 1930s. In spite of considerable activity in this field, the available experimental

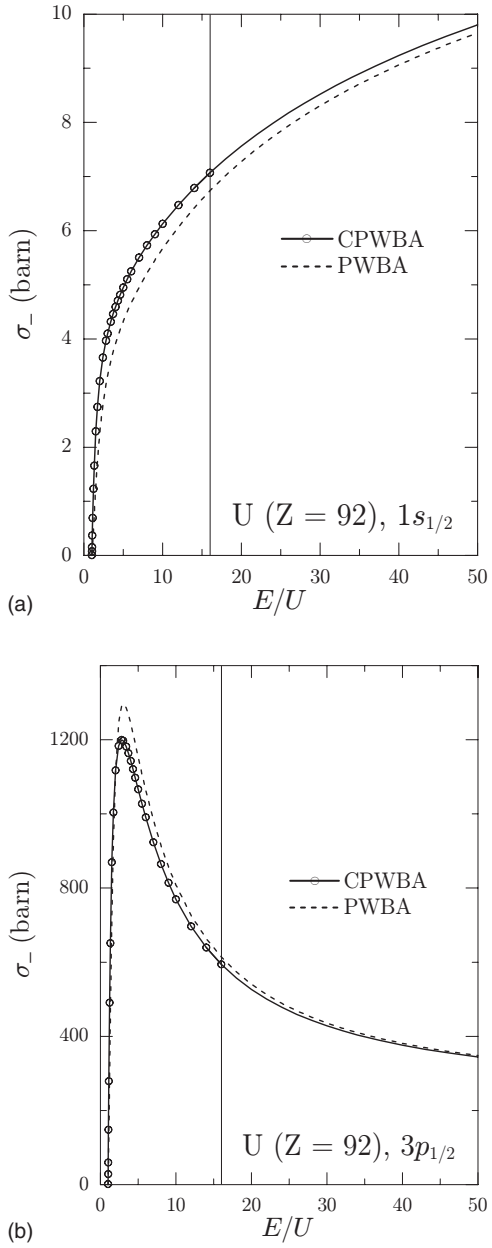

FIG. 5. Total cross sections for ionization of the *K*and *M*2 shells of uranium atoms by impact of electrons. Circles represent results from our numerical CPWBA calculation, Eq. (98). The continuous curves are the results from Eq. (99), and the dashed curves represent the PWBA cross sections, obtained by integrating the energy-loss DCS given by Eq. (76). The vertical lines mark the matching energy, $E=16U$.

information is still fairly limited, and insufficient for a quantitative assessment of the accuracy and limitations of the different theoretical approaches. Figure 6 shows cross sections for ionization of the *K* shell of the elements Al, Ar, Ti, Cr, Ni, and Ge. Calculations are seen to agree reasonably with the experiments and the agreement is better for the most recent measurements, which are also expected to be more accurate.

Figures 7 display calculated and measured cross sections for the *K* shell and *L* subshells of the elements Cu, Sr, Ag,

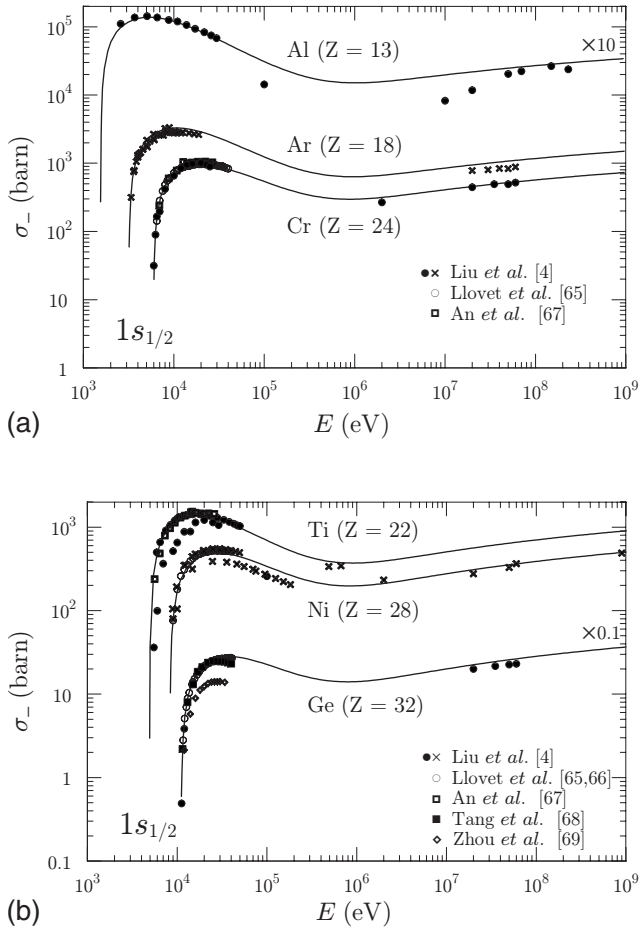

FIG. 6. Total cross sections for electron-impact ionization of the *K* shell of the elements Al, Ar, Ti, Cr, Ni, and Ge, as functions of the energy *E* of the projectile. Curves are the results from the CPWBA Eq. (99). Symbols represent experimental data; open circles [65,66], open squares [67], solid squares [68], and open diamonds [69] correspond to recent measurements. The solid circles and crosses are results from various groups (Refs. [70–89]), which were compiled by Liu *et al.* [4].

Xe, W, Au, Pb, and Bi. For the *K* shells, when there is enough experimental information available, the degree of agreement between theory and experiments is seen to be similar to that of the light elements shown in Fig. 6. In the case of *L* subshells, the comparison is not conclusive because of the considerable uncertainties of experimental data. This is partially due to the fact that ionization cross sections are derived from measured x-ray generation cross sections. In this derivation, use is made of fluorescence yields and Coster-Kronig coefficients which, in the case of *L* subshells, are affected by large uncertainties (of the order of 20% or larger; see, e.g., Ref. [90]).

As indicated above, published measured data for ionization of inner shells by impact of positrons are very rare. Figure 8 shows a comparison of calculated and experimental cross sections for positron impact ionization of the *K* shells of copper and silver atoms. Again, due to the scarcity of data, it is not possible to draw any conclusions from this comparison. Figure 8 also displays calculated cross sections for ion-

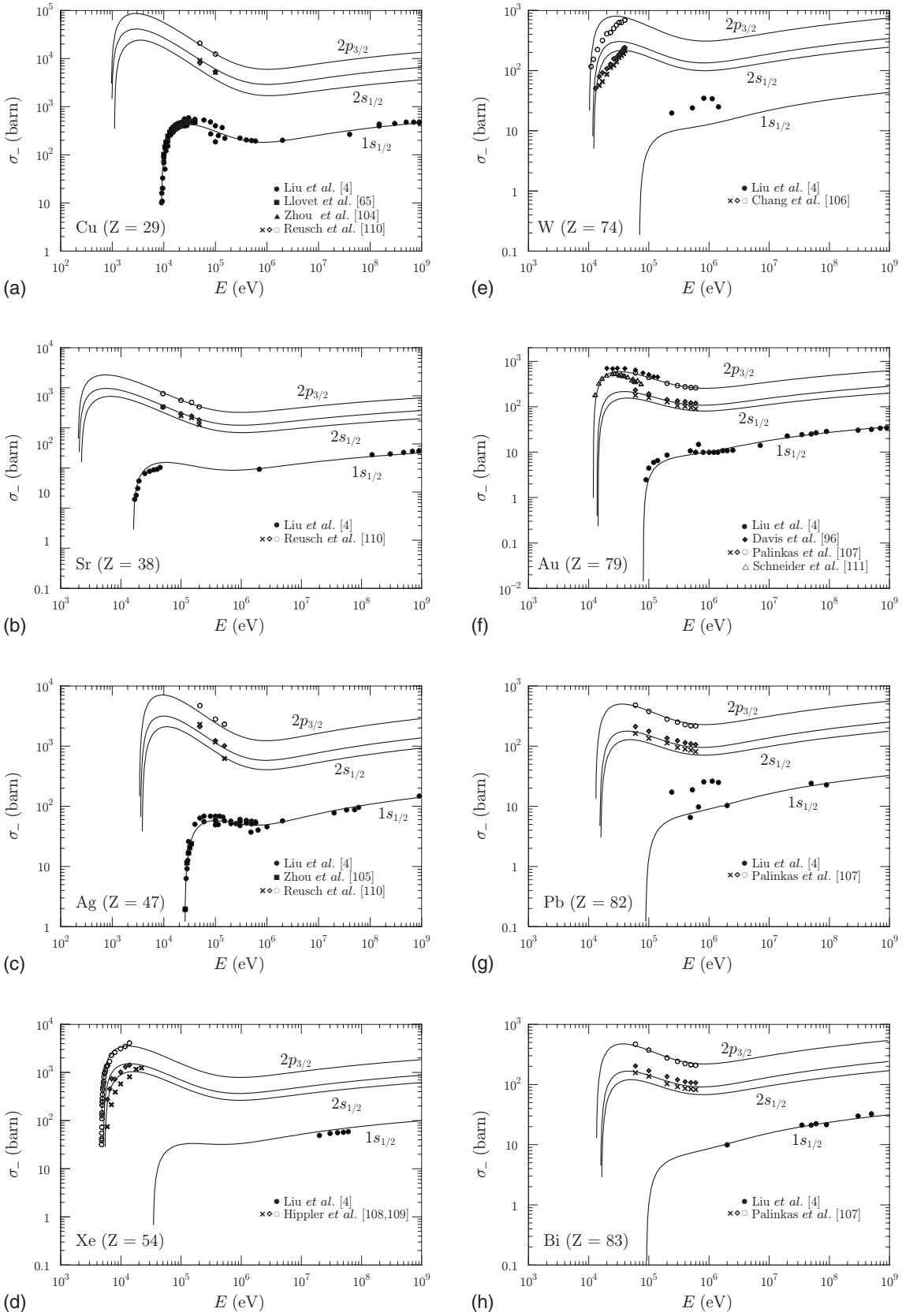

FIG. 7. Total cross sections for electron impact ionization of the K shell and L subshells of the elements Cu, Sr, Ag, Xe, W, Au, Pb, and Bi. Solid circles correspond to measurements for the K shell by different groups (see Refs. [79–89,91–103]), which were compiled by Liu *et al.* [4]. Other symbols correspond to recent measurements [65,104,105]. Experimental data for the L subshells are from Refs. [106–111]; crosses, diamonds, and open circles correspond to the $L1$, $L2$, and $L3$ subshells, respectively.

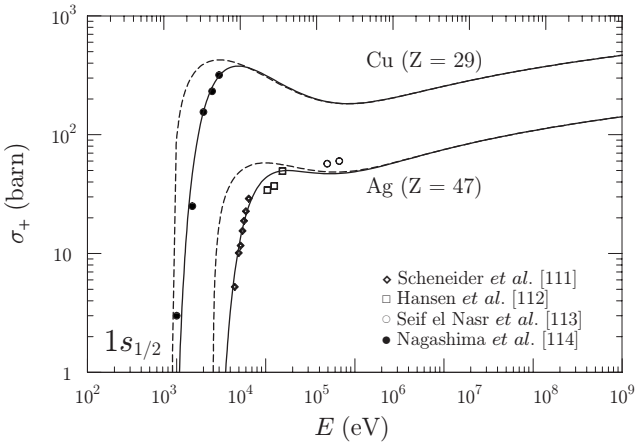

FIG. 8. Total cross sections for ionization of the K shell of the elements Cu and Ag by impact of positrons (solid curves) and electrons (dashed). Symbols represent experimental data for positrons [111–114].

ization of K shells by electron impact. At relatively low energies, the cross sections for electrons are seen to be substantially larger than those for positrons, the difference being due to the combined effect of exchange (which is not present for positrons) and of the opposite signs of the potentials experienced by electrons and positrons.

VII. CONCLUDING COMMENTS

The combined use of the semirelativistic DWBA and the PWBA proposed in the present paper provides a convenient theoretical description of inner-shell ionization by impact of electrons and positrons, which allows the calculation of realistic ionization cross sections of neutral atoms and positive ions from the ionization threshold up to arbitrarily large energies. We have performed accurate calculations of ionization cross sections using the PWBA. The DWBA has been used to calculate distortion and exchange corrections to the PWBA for an energy interval wide enough to allow smooth extrapolation to higher energies by using the fitted scaling factor $E/(E+bU)$. The proposed calculation scheme has been implemented in a set of computer codes, which have been used to generate an extensive database of ionization cross sections for the K shell, and the L and M subshells of all the elements between hydrogen ($Z=1$) and einstenium ($Z=99$) for electrons and positrons with energies from 50 eV up to 1 GeV. This database, which will be made available in due course, can be used to improve the description of x-ray generation by electrons and positrons in general-purpose Monte Carlo codes.

As a by-product of the present work, we have generated a database of both GOSs and TGOSs for K shells and L and M subshells of all elements. These GOSs may be useful to compute cross sections for ionization of neutral atoms by impact of muons, protons, and α particles. In particular, they may allow the systematic calculation of inner-shell corrections to the Bethe stopping-power formula for charged particles heavier than electrons.

ACKNOWLEDGMENTS

We are indebted to José M. Fernández-Varea, Michael Dingfelder, and Silvina Segui, for their collaboration in the early stages of this work, and to Mitio Inokuti for thoughtful advice and for his critical reading of a preliminary version of the manuscript. Our appreciation also to Xavier Llovet for enlightening discussions and comments, and for providing us with a wealth of experimental information and data. Financial support from the Spanish Ministerio de Educación y Ciencia (Project No. FPA2006-12066) is gratefully acknowledged. D.B. also acknowledges support from the Departament d'Universitats, Recerca i Societat de la Informació de la Generalitat de Catalunya and from the European Social Fund.

APPENDIX A: DIRAC WAVE FUNCTIONS

In this appendix we briefly review some specifics of the Dirac equation, set the notation, and present tools used in the theory sections. The Dirac Hamiltonian for an electron in a central field $V(r)$ is (see, i.e., Rose [115])

$$\mathcal{H}_{\mathrm{D}} = c\tilde{\boldsymbol{\alpha}}\cdot\mathbf{p} + \tilde{\beta}m_e c^2 + V(r), \tag{A1}$$

where $\mathbf{p}=-i\hbar\boldsymbol{\nabla}$ is the momentum operator, and $\tilde{\boldsymbol{\alpha}}$ and $\tilde{\beta}$ are the Dirac matrices. The standard representation for these matrices is

$$\tilde{\boldsymbol{\alpha}} = \begin{pmatrix} 0 & \boldsymbol{\sigma} \\ \boldsymbol{\sigma} & 0 \end{pmatrix}, \quad \tilde{\beta} = \begin{pmatrix} I_2 & 0 \\ 0 & -I_2 \end{pmatrix}, \tag{A2}$$

where $\boldsymbol{\sigma}$ stands for the familiar 2×2 Pauli spin matrices and I_2 is the 2×2 unit matrix. The time-independent Dirac wave equation takes the form

$$[c\tilde{\boldsymbol{\alpha}}\cdot\mathbf{p} + \tilde{\beta}m_e c^2 + V(r)]\psi(\mathbf{r}) = \mathcal{W}\psi(\mathbf{r}), \tag{A3}$$

where $\mathcal{W}$ is the (total) energy eigenvalue.

1. Plane waves

In the case of a free electron ($V\equiv 0$), the Hamiltonian (A1) commutes with the momentum operator and, hence, there exists a complete set of eigenfunctions $\phi_{\mathbf{k}i}(\mathbf{r})$ common to $\mathcal{H}_{\mathrm{D}}$ and $\mathbf{p}$. These are the plane waves

$$\phi_{\mathbf{k}\mu\tau}(\mathbf{r}) = \frac{e^{i\mathbf{k}\cdot\mathbf{r}}}{(2\pi)^{3/2}} U_{\mathbf{k}\mu\tau}, \tag{A4}$$

where the index τ ($=\pm 1$) denotes the sign of the energy, $\mu = \pm 1/2$, and $U_{\mathbf{k}\mu\tau}$ are the following double spinors:

$$U_{\mathbf{k},\mu,+1} = \left(1 + \frac{(c\hbar k)^2}{(|\mathcal{W}| + m_e c^2)^2}\right)^{-1/2} \begin{pmatrix} I_2 \\ \dfrac{c\hbar\boldsymbol{\sigma}\cdot\mathbf{k}}{|\mathcal{W}| + m_e c^2} \end{pmatrix} \chi_\mu, \tag{A5}$$

$$U_{\mathbf{k},\mu,-1} = \left(1 + \frac{(c\hbar k)^2}{(|\mathcal{W}| + m_e c^2)^2}\right)^{-1/2} \begin{pmatrix} -\dfrac{c\hbar\boldsymbol{\sigma}\cdot\mathbf{k}}{|\mathcal{W}| + m_e c^2} \\ I_2 \end{pmatrix} \chi_\mu, \tag{A6}$$

and

$$\chi_{+1/2} = \begin{pmatrix} 1 \\ 0 \end{pmatrix}, \quad \chi_{-1/2} = \begin{pmatrix} 0 \\ 1 \end{pmatrix}, \tag{A7}$$

are the Pauli unit spinors.

It can be easily verified that, for a given $\mathbf{k}$,

$$U^\dagger_{\mathbf{k}\mu'\tau'} U_{\mathbf{k}\mu\tau} = \delta_{\mu',\mu}\delta_{\tau',\tau} \quad \text{and} \quad \sum_{\mu,\tau} U_{\mathbf{k}\mu\tau} U^\dagger_{\mathbf{k}\mu\tau} = I_4. \tag{A8}$$

In principle, the present calculations involve only positive-energy (electron) states. Even in the case when the projectile is a positron, its spherical waves may be obtained by solving the radial equations (A11) for the electron with the sign of the potential reversed (as dictated by the charge conjugation transformation). However, in the formulation of the PWBA we make explicit use of the completeness of the plane-wave four-spinors through the usage of energy projection operators. For this aim, it is convenient to introduce the operator

$$\Pi_{\mathbf{k},+1} \equiv \sum_{\mu=\pm 1/2} U_{\mathbf{k},\mu,+1} U^\dagger_{\mathbf{k},\mu,+1} = \frac{1}{2|\mathcal{W}|}(|\mathcal{W}| + c\hbar\tilde{\boldsymbol{\alpha}}\cdot\mathbf{k} + \tilde{\beta} m_e c^2) \tag{A9}$$

It can be easily verified that $\Pi^2_{\mathbf{k},+1} = \Pi_{\mathbf{k},+1}$. Therefore, $\Pi_{\mathbf{k},+1}$ is a projection operator: it projects spinor states on the subspace of positive energy.

2. Spherical waves and distorted plane waves

Let us now consider an electron in a central field $V(r)$. The angular momentum operator for a Dirac particle is $\mathbf{J} = \mathbf{L} + \mathbf{S}$, where $\mathbf{L} = -i\mathbf{r}\times\boldsymbol{\nabla}$ is the orbital angular momentum and $\mathbf{S}$ is the spin angular momentum (all angular momenta are in units of $\hbar$). Since $\mathcal{H}_\mathrm{D}$ commutes with $\mathbf{J}^2$, J_z, and the parity operator ($\mathcal{P} = \tilde{\beta}\times$ space inversion), there exists a complete basis of eigenfunctions common to these four operators. These eigenfunctions are the spherical waves, and have the form [56,115]

$$\psi_{\epsilon\kappa m}(\mathbf{r}) = \frac{1}{r}\begin{pmatrix} P(r)\Omega_{\kappa,m}(\hat{\mathbf{r}}) \\ iQ(r)\Omega_{-\kappa,m}(\hat{\mathbf{r}}) \end{pmatrix}. \tag{A10}$$

where $\Omega_{\kappa,m}(\hat{\mathbf{r}})$ are spherical spinors, and $P(r)$ and $Q(r)$ are the large- and small-component radial functions, which satisfy the coupled differential equations

$$\frac{dP}{dr} = -\frac{\kappa}{r}P + \frac{\epsilon - V + 2m_e c^2}{c\hbar}Q,$$

$$\frac{dQ}{dr} = -\frac{\epsilon - V}{c\hbar}P + \frac{\kappa}{r}Q, \tag{A11}$$

where $\epsilon = \mathcal{W} - m_e c^2$ is the electron energy, exclusive of its rest energy. The spherical spinors are eigenfunctions of the total angular momentum in Pauli's theory, and are given by

$$\Omega_{\kappa,m}(\hat{\mathbf{r}}) \equiv \sum_{\mu=\pm 1/2} \langle \ell, 1/2, m-\mu, \mu | j, m\rangle Y_{\ell,m-\mu}(\hat{\mathbf{r}})\chi_\mu, \tag{A12}$$

where the quantities $\langle \ell, 1/2, m-\mu, \mu | j, m\rangle$ are Clebsch-Gordan coefficients and $Y_{\ell m}(\hat{\mathbf{r}})$ are spherical harmonics. To simplify notation, it is customary to introduce the relativistic angular momentum quantum number

$$\kappa = (\ell - j)(2j + 1), \tag{A13}$$

which specifies both the total angular momentum $[j]$ and the parity $[(-1)^\ell]$ of the Dirac spherical wave,

$$j = |\kappa| - \frac{1}{2}, \quad \ell = j + \frac{\kappa}{2|\kappa|}. \tag{A14}$$

The potentials occurring in the present calculations are combinations of a short-range field and a Coulomb field,

$$V(r) = V_\mathrm{sr} + \frac{Z_\infty e^2}{r}, \tag{A15}$$

where the short-range component is assumed to vanish for $r > r_\mathrm{c}$. Thus, for the DFS field of neutral atoms, r_c is the onset of the Latter tail [38,39] and $Z_\infty = -1$. Radial functions for these potentials can be calculated numerically to high accuracy by using the subroutine package RADIAL [57]. The numerical algorithm implemented in these subroutines combines a cubic-spline interpolation of the function $rV(r)$ with local power-series expansions of the radial functions in such a way that truncation errors are effectively reduced. Nevertheless, the original subroutines had to be further optimized to render the present calculations possible. In the case of bound orbitals ($\epsilon < 0$), each discrete energy level is characterized by the principal quantum number n and the relativistic quantum number κ. Bound orbitals calculated by RADIAL are normalized to unity and, therefore, the calculated orbitals satisfy the orthonormality relation

$$\int \psi^\dagger_{n'\kappa'm'}(\mathbf{r})\psi_{n\kappa m}(\mathbf{r})d\mathbf{r} = \delta_{n'n}\delta_{\kappa'\kappa}\delta m' m. \tag{A16}$$

The radial functions of free spherical waves (with $\epsilon > 0$) are normalized in such a way that the large-component radial function asymptotically oscillates with unit amplitude,

$$P(r) \underset{r\to\infty}{\sim} \sin\left(kr - \ell\frac{\pi}{2} - \eta \ln 2kr + \delta_{\epsilon\kappa}\right), \tag{A17}$$

where

$$k = (c\hbar)^{-1}\sqrt{\epsilon(\epsilon + 2m_e c^2)} \tag{A18}$$

is the wave number and $\eta = Z_\infty e^2 m_e/(\hbar^2 k)$ is the Sommerfeld parameter. The phase shift $\delta_{\epsilon\kappa}$ is determined numerically by integrating the radial equations from $r = 0$ outward to a point

further than the range r_c of the $V_{\rm sr}$ potential, and matching the result at that point to a combination of the regular and irregular Dirac-Coulomb functions. The package RADIAL implements efficient algorithms for the calculation of Dirac-Coulomb wave functions. In the limit $Z_\infty=0$, the radial Dirac-Coulomb functions reduce to Bessel functions and, therefore, the generic algorithm is also valid for finite-range fields. Free spherical waves normalized in the form (A17) satisfy the orthogonality relation

$$\int \psi^\dagger_{\epsilon'\kappa'm'}(\mathbf{r})\psi_{\epsilon\kappa m}(\mathbf{r})\mathrm{d}\mathbf{r} = \frac{\epsilon}{k}\pi\delta(\epsilon'-\epsilon)\delta_{\kappa'\kappa}\delta_{m'm}. \tag{A19}$$

In collision theory, states of free particles in the initial and final channels are described as distorted plane waves, i.e., by solutions of the Dirac equation for the potential $V(r)$ that asymptotically behave as a plane wave plus an outgoing (+) or incoming (−) spherical wave. A DPW is characterized by the wave vector $\mathbf{k}$ and spin μ; it can be expanded in the basis of spherical waves as [115]

$$\psi^{(\pm)}_{\mathbf{k}\mu}(\mathbf{r}) = \frac{1}{k}\sqrt{\frac{\epsilon+2m_ec^2}{\pi(\epsilon+m_ec^2)}}\sum_{\kappa,m} i^\ell \exp(\pm \mathrm{i}\delta_\kappa) \times\{[\Omega_{\kappa m}(\hat{\mathbf{k}})]^\dagger\chi_\mu\}\psi_{\epsilon\kappa m}(\mathbf{r}) \tag{A20}$$

where

$$\epsilon = \sqrt{(c\hbar k)^2+(m_ec^2)^2}-m_ec^2 \tag{A21}$$

is the kinetic energy of the particle. It can be easily verified that, with the adopted normalization for free spherical waves, the DPWs satisfy the orthogonality relation

$$\int [\psi^{(\pm)}_{\mathbf{k}'\mu'}(\mathbf{r})]^\dagger\psi^{(\pm)}_{\mathbf{k}\mu}(\mathbf{r})d\mathbf{r} = \delta(\mathbf{k}'-\mathbf{k})\delta_{\mu'\mu}. \tag{A22}$$

In the limit where the strength of the potential tends to zero ($V=0$), the phase shifts vanish and the radial functions of free states ($E>0$) reduce to regular spherical Bessel functions

$$P^{(0)}_{\epsilon\kappa}(r) = krj_\kappa(kr), \quad Q^{(0)}_{\epsilon\kappa}(r) = \sqrt{\frac{\epsilon}{\epsilon+2m_ec^2}}krj_{\kappa-1}(kr) \quad \text{if } \kappa>0,$$

$$P^{(0)}_{\epsilon\kappa}(r) = krj_{-\kappa-1}(kr), \quad Q^{(0)}_{\epsilon\kappa}(r) = -\sqrt{\frac{\epsilon}{\epsilon+2m_ec^2}}krj_{-\kappa}(kr) \quad \text{if } \kappa<0. \tag{A23}$$

In a more compact form, valid for any κ,

$$P^{(0)}_{\epsilon\kappa}(r) = krj_\ell(kr), \quad Q^{(0)}_{\epsilon\kappa}(r) = \frac{\kappa}{|\kappa|}\sqrt{\frac{\epsilon}{\epsilon+2m_ec^2}}krj_{\bar{\ell}}(kr), \tag{A24}$$

where

$$\bar{\ell} = \begin{cases} -\kappa & \text{if } \kappa<0, \\ \kappa-1 & \text{if } \kappa>0, \end{cases} \tag{A25}$$

is the value of ℓ corresponding to $-\kappa$. Note that, in the $V=0$ limit, the DPW reduces to the positive-energy plane wave, $\psi^{(\pm)}_{\mathbf{k}\mu}(\mathbf{r})\to\phi_{\mathbf{k},\mu,+1}(\mathbf{r})$.

[1] F. Salvat, J. M. Fernández-Varea, and J. Sempau, computer code PENELOPE-2006 (OECD/NEA Data Bank, Issy-les-Moulineaux, France, 2006), http://www.nea.fr/lists/penelope.html
[2] X-5 Monte Carlo Team, Los Alamos National Laboratory, Los Alamos, NM, Report No. LA-UR-03-1987, 2003 (unpublished).
[3] I. Kawrakow and D. W. O. Rogers, National Research Council of Canada, Ottawa, Report No. PIRS-701, 2001 (unpublished).
[4] M. Liu, Z. An, C. Tang, Z. Liu, X. Peng, and X. Long, At. Data Nucl. Data Tables **76**, 213 (2000).
[5] E. Casnati, A. Tartari, and C. Baraldi, J. Phys. B **15**, 155 (1982).
[6] W. Lotz, Z. Phys. **232**, 101 (1970).
[7] C. Hombourger, J. Phys. B **31**, 3693 (1998).
[8] A. K. F. Haque, M. A. Uddin, A. K. Basak, K. R. Karim, and B. C. Saha, Phys. Rev. A **73**, 012708 (2006).
[9] C. J. Powell, Rev. Mod. Phys. **48**, 33 (1976).
[10] C. J. Powell, in *Electron Impact Ionization*, edited by T. D. Märk and G. H. Dunn (Springer Verlag, New York, 1985), pp. 198–231.
[11] P. Rez, J. Res. Natl. Inst. Stand. Technol. **107**, 487 (2002).
[12] J. H. Scofield, Phys. Rev. A **18**, 963 (1978).
[13] Y. K. Kim and M. E. Rudd, Phys. Rev. A **50**, 3954 (1994).
[14] Y. K. Kim, J. P. Santos, and F. Parente, Phys. Rev. A **62**, 052710 (2000).
[15] J. P. Santos, F. Parente, and Y. K. Kim, J. Phys. B **36**, 4211 (2003).
[16] H. Deutsch, K. Becker, and T. D. Märk, Int. J. Mass Spectrom. **177**, 47 (1998).
[17] H. Kolbenstvedt, J. Appl. Phys. **38**, 4785 (1967).
[18] S. M. Seltzer, in *Monte Carlo Transport of Electrons and Photons*, edited by T. Jenkins, W. Nelson, and A. Rindi (Plenum Press, New York, 1989), pp. 103–110.
[19] R. Mayol and F. Salvat, J. Phys. B **23**, 2117 (1990).
[20] F. Bell, J. Phys. B **22**, 287 (1989).
[21] W. Nakel and C. T. Whelan, Phys. Rep. **315**, 409 (1999).
[22] H. Ruoff and W. Nakel, J. Phys. B **20**, 2299 (1987).
[23] H. Ehrhardt, K. H. Hesselbacher, K. Jung, M. Schulz, and K. Willmann, J. Phys. B **5**, 2107 (1972).
[24] S. Keller, C. T. Whelan, H. Ast, H. R. J. Walters, and R. M. Dreizler, Phys. Rev. A **50**, 3865 (1994).
[25] A. Prideaux, D. H. Madison, and K. Bartschat, Phys. Rev. A **72**, 032702 (2005).

[26] M. S. Pindzola, D. L. Moores, and D. C. Griffin, Phys. Rev. A **40**, 4941 (1989).
[27] C. J. Fontes, D. H. Sampson, and H. L. Zhang, Phys. Rev. A **47**, 1009 (1993).
[28] D. H. Sampson, Phys. Rev. A **34**, 986 (1986).
[29] H. L. Zhang, D. H. Sampson, and A. K. Mohanty, Phys. Rev. A **40**, 616 (1989).
[30] S. Segui, M. Dingfelder, and F. Salvat, Phys. Rev. A **67**, 062710 (2003).
[31] J. Colgan, C. J. Fontes, and H. L. Zhang, Phys. Rev. A **73**, 062711 (2006).
[32] H. Bethe, in *Quantentheorie*, edited by H. Geiger and K. Scheel, Handbuch der Physik Vol. 24/1 (Springer, Berlin, 1933), pp. 273–560.
[33] U. Fano, Annu. Rev. Nucl. Sci. **13**, 1 (1963).
[34] M. Inokuti, Rev. Mod. Phys. **43**, 297 (1971).
[35] V. I. Ochkur, Sov. Phys. JETP **20**, 1175 (1965).
[36] M. R. H. Rudge, Rev. Mod. Phys. **40**, 564 (1968).
[37] Y. K. Kim, Phys. Rev. A **64**, 032713 (2001).
[38] R. Latter, Phys. Rev. **99**, 510 (1955).
[39] D. Liberman, D. T. Cromer, and J. T. Waber, Phys. Rev. **137**, A27 (1965).
[40] T. A. Carlson, *Photoelectron and Auger Spectroscopy* (Plenum Press, New York, 1975).
[41] C. J. Joachain, *Quantum Collision Theory* (North-Holland, Amsterdam, 1983).
[42] P. A. Lee, P. H. Citrin, P. Eisenberger, and B. M. Kincaid, Rev. Mod. Phys. **53**, 769 (1981).
[43] R. M. Sternheimer, S. M. Seltzer, and M. J. Berger, Phys. Rev. B **26**, 6067 (1982).
[44] M. Inokuti and D. Y. Smith, Phys. Rev. B **25**, 61 (1982).
[45] H. Bethe, Z. Phys. **76**, 293 (1932).
[46] P. Schattschneider, C. Hébert, H. Franco, and B. Jouffrey, Phys. Rev. B **72**, 045142 (2005).
[47] W. Heitler, *The Quantum Theory of Radiation* (Dover Publications, New York, 1953).
[48] W. Greiner and J. Reinhardt, *Quantum Electrodynamics* (Springer, Berlin, 1994).
[49] H. Bethe, Ann. Phys. (Leipzig) **397**, 325 (1930).
[50] S. M. Cohen, Phys. Rev. A **68**, 042704 (2003).
[51] R. H. Romero and G. A. Aucar, Phys. Rev. A **57**, 2212 (1998).
[52] A. R. Edmonds, *Angular Momentum in Quantum Mechanics* (Princeton University Press, Princeton, NJ, 1957).
[53] *Handbook of Mathematical Functions*, edited by M. Abramowitz and I. A. Stegun (Dover, New York, 1964).
[54] J. B. Mann and W. R. Johnson, Phys. Rev. A **4**, 41 (1971).
[55] V. B. Berestetskii and A. I. Akhiezer, *Quantum Electrodynamics* (Interscience, New York, 1965).
[56] I. P. Grant, Proc. Phys. Soc. London **86**, 523 (1965).
[57] F. Salvat, J. M. Fernández-Varea, and W. Williamson, Jr., Comput. Phys. Commun. **90**, 151 (1995).
[58] S. Segui, M. Dingfelder, J. M. Fernández-Varea, and F. Salvat, J. Phys. B **35**, 33 (2002).
[59] C. Møller, Ann. Phys (Leipzig) **406**, 531 (1932).
[60] H. J. Bhabha, Proc. R. Soc. London, Ser. A **154**, 195 (1936).
[61] F. Rohrlich and B. C. Carlson, Phys. Rev. **93**, 38 (1954).
[62] ICRU, *Stopping Powers for Electrons and Positrons*, Report No. 37 (ICRU, Bethesda, MD, 1984).
[63] C. Merlet, X. Llovet, and J. M. Fernández-Varea, Phys. Rev. A **73**, 062719 (2006).
[64] C. S. Campos, M. A. Z. Vasconcellos, X. Llovet, and F. Salvat, Phys. Rev. A **66**, 012719 (2002).
[65] X. Llovet, C. Merlet, and F. Salvat, J. Phys. B **33**, 3761 (2000).
[66] C. Merlet, X. Llovet, and F. Salvat, Phys. Rev. A **69**, 032708 (2004).
[67] Z. An, M. T. Liu, Y. C. Fu, Z. M. Luo, C. H. Tang, C. M. Li, B. H. Zhang, and Y. J. Tang, Nucl. Instrum. Methods Phys. Res. B **207**, 268 (2003).
[68] C. Tang, Z. An, Z. Luo, and M. Liu, J. Appl. Phys. **91**, 6739 (2002).
[69] C. Zhou, Z. An, and Z. Luo, J. Phys. B **35**, 841 (2002).
[70] A. E. Smick and P. Kirkpatrick, Phys. Rev. **67**, 153 (1945).
[71] L. T. Pockman, D. L. Webster, P. Kirkpatrick, and K. Harworth, Phys. Rev. **71**, 330 (1947).
[72] W. Hink and A. Ziegler, Z. Phys. **226**, 222 (1969).
[73] H. Tawara, K. G. Harrison, and F. J. De Heer, Physica **63**, 351 (1973).
[74] J. Jessenberger and W. Hink, Z. Phys. A **275**, 331 (1975).
[75] M. Kamiya, A. Kuwako, K. Ishii, S. Morita, and M. Oyamada, Phys. Rev. A **22**, 413 (1980).
[76] R. Hippler, K. Saeed, I. McGregor, and H. Kleinpoppen, Z. Phys. A **307**, 83 (1982).
[77] C. Quarles and M. Semaan, Phys. Rev. A **26**, 3147 (1982).
[78] H. Platten, G. Schiwietz, and G. Nolte, Phys. Lett. **107A**, 83 (1985).
[79] S. C. McDonald and B. M. Spicer, Phys. Rev. A **37**, 985 (1988).
[80] W. Scholz, A. Li-Scholz, R. Collé, and L. Preiss, Phys. Rev. Lett. **29**, 761 (1972).
[81] S. A. H. Seif el Nasr, D. Berényi, and G. Bibok, Z. Phys. **267**, 169 (1974).
[82] K. Ishii, M. Kamiya, K. Sera, S. Morita, H. Tawara, M. Oyamada, and T. C. Chu, Phys. Rev. A **15**, 906 (1977).
[83] D. H. H. Hoffmann, C. Brendel, H. Genz, W. Löw, S. Müller, and A. Richter, Z. Phys. A **293**, 187 (1979).
[84] D. H. H. Hoffmann, H. Genz, W. Löw, and A. Richter, Phys. Lett. **65A**, 304 (1979).
[85] K. Shima, T. Nakagawa, K. Umetani, and T. Mikumo, Phys. Rev. A **24**, 72 (1981).
[86] H. Genz, C. Brendel, P. Eschwey, U. Kuhn, W. Löw, A. Richter, and P. Seserko, Z. Phys. A **305**, 9 (1982).
[87] G. L. Westbrook and C. A. Quarles, Nucl. Instrum. Methods Phys. Res. B **24-25**, 196 (1987).
[88] Z. M. Luo, Z. An, F. He, T. Li, X. Long, and X. Peng, J. Phys. B **29**, 4001 (1996).
[89] F. Q. He, X. F. Peng, X. G. Long, Z. M. Luo, and Z. An, Nucl. Instrum. Methods Phys. Res. B **129**, 445 (1997).
[90] M. O. Krause, J. Phys. Chem. Ref. Data **8**, 307 (1979).
[91] H. Hansen, H. Weigmann, and A. Flammersfeld, Nucl. Phys. **58**, 241 (1964).
[92] D. H. Rester and W. E. Dance, Phys. Rev. **152**, 1 (1966).
[93] K. H. Berkner, S. N. Kaplan, and R. V. Pyle, Bull. Am. Phys. Soc. **15**, 786 (1970).
[94] L. M. Middleman, R. L. Ford, and R. Hofstadter, Phys. Rev. A **2**, 1429 (1970).
[95] H. Hubner, K. Ilgen, and K. W. Hoffmann, Z. Phys. **255**, 269 (1972).
[96] D. V. Davis, V. D. Mistry, and C. A. Quarles, Phys. Lett. **38A**, 169 (1972).

[97] B. Schlenk, D. Berényi, S. Ricz, A. Valek, and G. Hock, Acta Physiol. Hung. **41**, 159 (1976).
[98] S. Ricz, B. Schlenk, D. Berényi, G. Hock, and A. Valek, Acta Phys. Hung. **42**, 269 (1977).
[99] D. Berényi, G. Hock, S. Ricz, B. Schlenk, and A. Valek, J. Phys. B **11**, 709 (1978).
[100] K. Shima, Phys. Lett. **77A**, 237 (1980).
[101] K. Kiss, G. Kalman, J. Pálinkás, and B. Schlenk, Acta Phys. Hung. **50**, 97 (1981).
[102] V. P. Shevelko, A. M. Solomon, and V. S. Vukstich, Phys. Scr. **43**, 158 (1991).
[103] Z. An, T. H. Li, L. M. Wang, X. Y. Xia, and Z. M. Luo, Phys. Rev. A **54**, 3067 (1996).
[104] C. G. Zhou, Z. An, and Z. M. Luo, Chin. Phys. Lett. **18**, 759 (2001).
[105] C. G. Zhou, Y. C. Fu, Z. An, C. H. Tang, and Z. M. Luo, Chin. Phys. Lett. **18**, 531 (2001).
[106] C. N. Chang, Phys. Rev. A **19**, 1930 (1979).
[107] J. Pálinkás and B. Schlenk, Z. Phys. A **297**, 29 (1980).
[108] R. Hippler, I. McGregor, M. Aydinol, and H. Kleinpoppen, Phys. Rev. A **23**, 1730 (1981).
[109] R. Hippler, H. Klar, K. Saeed, I. McGregor, H. Kleinpoppen, and A. J. Duncan, J. Phys. B **16**, L617 (1983).
[110] S. Reusch, H. Genz, W. Low, and A. Richter, Z. Phys. D: At., Mol. Clusters **3**, 379 (1986).
[111] H. Schneider, I. Tobehn, F. Ebel, and R. Hippler, Phys. Rev. Lett. **71**, 2707 (1993).
[112] H. Hansen and A. Flammersfeld, Nucl. Phys. **79**, 135 (1966).
[113] S. A. H. Seif el Nasr, D. Berényi, and G. Bibok, Z. Phys. A: Hadrons Nucl. **271**, 207 (1974).
[114] Y. Nagashima, F. Saito, Y. Itoh, A. Goto, and T. Hyodo, Phys. Rev. Lett. **92**, 223201 (2004).
[115] M. E. Rose, *Relativistic Electron Theory* (John Wiley and Sons, New York, 1961).